JOURNAL OF PETROLOGY | VOLUME 52 | NUMBER 6 | PAGES 1207–1236 | 2011 | doi:10.1093/petrology/egr025

Internal and External Fluid Sources for Eclogite-facies Veins in the Monviso Meta-ophiolite, Western Alps: Implications for Fluid Flow in Subduction Zones

CARL SPANDLER[1]*, THOMAS PETTKE[1] AND DANIELA RUBATTO[2]

[1]INSTITUTE OF GEOLOGICAL SCIENCES, UNIVERSITY OF BERN, BERN, CH-3012, SWITZERLAND

[2]RESEARCH SCHOOL OF EARTH SCIENCES, AUSTRALIAN NATIONAL UNIVERSITY, CANBERRA, ACT, 0200, AUSTRALIA

RECEIVED DECEMBER 17, 2009; ACCEPTED APRIL 28, 2011
ADVANCE ACCESS PUBLICATION JUNE 3, 2011

To contribute to our understanding of the mechanisms and pathways of fluid movement through deeply subducted crust, we investigate high-pressure veins cutting eclogite-facies (~2·0 GPa and ~600°C) metagabbros of the Monviso Ophiolite, Italian Western Alps. The veins consist mainly of omphacite with minor garnet, rutile, talc and accessory zircon. Most of the vein minerals have major and trace element compositions that are comparable with the host-rock minerals, and vein and host-rock zircons have similar Hf isotopic compositions. These observations support the conclusions of previous studies that these veins largely formed from a locally sourced hydrous fluid during prograde or peak metamorphism. However, the bulk-rock Cr and Ni contents of the veins are significantly higher than those of the surrounding host eclogites. We also document distinct Cr-rich (up to weight per cent levels) zones in omphacite, garnet and rutile in some vein samples. Vein garnet and talc also have relatively high MgO and Ni contents. X-ray maps of vein garnet and rutile grains reveal complex internal zoning features, which are largely defined by micrometre-scale variations in Cr content. Some grains have concentric and oscillatory zoning in Cr, whereas others feature a chaotic fracture-like pattern. These Cr-rich zones are associated with high concentrations of Ni, B, As, Sb, Nb, Zr and high ratios of light rare earth elements (LREE) to middle REE (MREE) compared with low-Cr vein and host-rock minerals. Petrological and mass-balance constraints verify that the Cr-rich zones in the veins were not derived from internally sourced fluids, but represent precipitates from an external fluid. The external source that is consistent with the distinctive trace element characteristics of the vein components is antigorite serpentinite, which forms the structural basement of the high-pressure metagabbros. We propose at least two separate growth mechanisms for the Monviso veins. Most vein infillings were formed during progressive prograde metamorphism from locally derived fluid. Influx of the serpentinite-derived or other external fluid was transient and episodic and was probably achieved via brittle fractures, which preferentially formed along the pre-existing vein structures. The dehydration of serpentinite at high pressures in subduction zones may provide crucial volatiles and trace elements for arc magmas. Our results indicate that the movement of these fluids through subducted oceanic crust is likely to be highly channeled and transient so the progressive development of vein systems in mafic rocks may also be crucial for forming channelways for long-distance fluid flow at depth in subduction zones.

KEY WORDS: *eclogite; fluid; Monviso; serpentinite; subduction; veins*

INTRODUCTION

Fluid flow through crustal rocks represents one of the most important processes governing mass and heat transfer in the Earth. In particular, the fluids produced by mineral dehydration in subducting plates are thought to be crucial for instigating mantle melting and the production of arc magmas (e.g. Peacock, 1993; Schmidt & Poli, 1998; Stern, 2002). Fluid movement in the slab at depth is also invoked as the principal source of intermediate-depth intra-slab earthquakes (Peacock, 2001; Hacker *et al.*, 2003). Quantification of the composition, evolution and flow of

*Corresponding author. Present address: School of Earth and Environmental Sciences, James Cook University, Townsville, QLD, 4811, Australia. E-mail: Carl.Spandler@jcu.edu.au

fluids in subduction zones concerns many aspects of the Earth Sciences.

The most important sources of fluids in subduction zones are expected to be devolatilizing mafic oceanic crust and serpentinite (Ulmer & Trommsdorff, 1999; Poli & Schmidt, 2002). However, direct evidence of high-pressure (HP) serpentinite dehydration is rarely preserved in the rock record. Recent experimental efforts have made progress in characterizing the chemistry of fluids at high pressure and temperature (e.g. Manning, 2004; Kessel *et al.*, 2005; Spandler *et al.*, 2007; Hermann & Spandler, 2008; Klimm *et al.*, 2008), but relatively little is known of how fluids migrate through, or react with, subducting slabs at depth (see Scambelluri & Philippot, 2001; Hermann *et al.*, 2006; Zack & John, 2007).

Exhumed HP and ultrahigh-pressure (UHP) metamorphic rocks represent fragments of previously subducted lithosphere and, hence, may be studied to gain insights into deep subduction-zone processes. Evidence that fluids flowed through these rocks at high pressure is preserved as cross-cutting veins that comprise eclogite-facies mineral assemblages (e.g. Philippot, 1993; Scambelluri *et al.*, 1998; Becker *et al.*, 1999; Rubatto & Hermann, 2003; Spandler & Hermann, 2006; Gao *et al.*, 2007; John *et al.*, 2008). A comprehensive understanding of how such veins form is yet to be reached, as these veins often have complex growth histories and many properties of fluids under high pressures are poorly known. Nevertheless, careful study can reveal important information on the source, composition and evolution of the fluids that formed the veins and, hence, can provide insights into the fluid flow regimes in subduction zones.

Perhaps the most extensively studied examples of HP veining in eclogitic rocks occur within the Monviso Ophiolite of the Western Alps, Italy. The Monviso Ophiolite represents a relatively coherent section of oceanic crust, which was subducted during the Tertiary (Lombardo *et al.*, 1978, 2002; Rubatto & Hermann, 2003). Within metagabbroic rocks are omphacite-rich veins, which have been the subject of detailed structural and petrological (Philippot, 1987; Philippot & Kienast, 1989; Philippot & van Roermund, 1992), fluid inclusion (Philippot & Selverstone, 1991; Nadeau *et al.*, 1993), stable isotope (Nadeau *et al.*, 1993), geochronological (Rubatto & Hermann, 2003) and geochemical (Philippot & Selverstone, 1991; Rubatto & Hermann, 2003) studies. The general consensus reached by these studies is that the veins formed as precipitates of locally derived hydrous fluid during ductile deformation at high pressure.

In this contribution, we build on the previous wealth of information on these veins by providing new textural evidence, bulk-rock and mineral major and trace element geochemistry, and zircon Hf isotope data on vein and host-rock samples from the Monviso Ophiolite. We focus on anomalous Cr-rich zones within vein minerals in an attempt to better constrain the sources of the fluid responsible for vein formation. Our new results indicate that vein formation is significantly more complex than indicated by previous models and, hence, provide new insights into the mechanisms of fluid flow through subducting crust. This work may also ultimately contribute to a better understanding of mass transfer and seismicity in subduction zones.

GEOLOGICAL SETTING

The Monviso Ophiolite is a 35 km long, 8 km wide north–south-trending complex that is tectonically sandwiched between the Queyras sedimentary Unit (Schistes Lustrés) to the west and the Dora Maira continental unit to the east. Detailed geological descriptions and maps of the ophiolite have been published elsewhere (e.g. Lombardo *et al.*, 1978; MONVISO, 1980; Schwartz *et al.*, 2000), hence, here we present only a geological overview of the region. The Monviso complex consists of a series of serpentinite, metagabbro and metabasalt units with subordinate mica- and calc-schist (Lombardo *et al.*, 1978, 2002). Serpentinite is the dominant rock type of the complex (Schwartz *et al.*, 2001). The entire sequence originally formed part of the Jurassic western Tethys oceanic lithosphere, which was subsequently subducted and metamorphosed under eclogite-facies conditions during the Tertiary (Lombardo *et al.*, 1978, 2002; Cliff *et al.*, 1998; Rubatto & Hermann, 2003). Conditions of metamorphism vary from unit to unit, which indicates that the current arrangement of some units may have occurred only during the rapid exhumation ($\sim$1 cm a^{-1}) of the massif (Schwartz *et al.*, 2000, 2001).

The samples examined in this study derive from the Lago Superiore Unit in the central part of the complex (see Lombardo *et al.*, 1978; Schwartz *et al.*, 2000). The Lago Superiore Unit consists of highly deformed Mg–Al and Fe–Ti metagabbros and talc schists, which are structurally underlain by antigorite serpentinites. The presence of rodingite dykes in the serpentinite body and oxygen isotope compositions of the metagabbros indicate that these rocks underwent hydration and alteration at, or near, the seafloor, prior to subduction (Nadeau *et al.*, 1993; Philippot *et al.*, 1998; Lombardo *et al.*, 2002). Continuity of structural fabrics (Schwartz *et al.*, 2000), serpentine mineralogy (Auzende *et al.*, 2006), the presence of eclogitic blocks within the serpentinite unit (Blake *et al.*, 1995) and widespread retrograde overprinting features (Blake *et al.* 1995; Schwartz *et al.*, 2000) indicate that both metagabbro and serpentinite units experienced similar conditions of eclogite-facies metamorphism and subsequent exhumation. However, the present contact between the eclogitic metagabbros and serpentinites is mapped as tectonic (Lombardo *et al.*, 1978), which testifies to some structural displacement of the original lithostratigraphic sequence.

The serpentinite unit is a 400 m thick mélange containing subordinate blocks of metarodingite, eclogite and metagabbro set within foliated serpentinite (Lombardo *et al.*, 1978; MONVISO, 1980; Blake *et al.*, 1995). The serpentinite consists mainly of HP antigorite (Auzende *et al.*, 2006), magnetite and chlorite, but may also contain minor amounts of tremolite, talc, titanian clinohumite, brucite and carbonate. The protolith can be recognized as lherzolite with minor harzburgite and dunite (MONVISO, 1980), despite almost complete alteration of relict mantle minerals. Rare veins containing olivine and/or chrysotile have been reported cutting the serpentinite from several localities (Compagnoni *et al.*, 1985; Groppo & Compagnoni, 2007). The olivine-bearing veins have been interpreted as precipitation products from fluids produced by brucite dehydration reactions under HP metamorphic conditions (Groppo & Compagnoni, 2007).

Both metagabbro types represent mafic cumulates that underwent peak metamorphic conditions of around 600°C and 1·9–2·4 GPa (Messiga *et al.*, 1999; Schwartz *et al.*, 2000), followed by partial blueschist- and greenschist-facies overprinting during exhumation (Lardeaux *et al.*, 1987). The Mg–Al metagabbros preserve a peak metamorphic mineral assemblage of Cr-rich omphacite ('smaragdite'), epidote, garnet, talc, rutile and occasionally, Cr-rich magnesiochloritoid (Lardeaux *et al.*, 1987; Messiga *et al.*, 1999). The mylonitic Fe–Ti metagabbros form metre- to tens of metre-scale pods or lenses within the Mg–Al metagabbros (Philippot & van Roermund, 1992). The Fe–Ti metagabbros are Cr poor and comprise a classic eclogite-facies mineral paragenesis of omphacite, garnet, rutile, quartz, apatite and accessory zircon (Lardeaux *et al.*, 1987; Philippot, 1987; Philippot & Kienast, 1989). Phengite, pyrite and glaucophane may also be present in minor amounts.

Two principal vein types cut the Fe–Ti eclogites (Philippot, 1987; Philippot & Kienast, 1989). Type-1 veins or segregations (millimetres to centimetres thick) are little deformed tension gashes and dilatational fractures, which consist almost solely of fibrous omphacite (Fig. 1a). Type-1 veins are interpreted to be contemporaneous with the mylonitic deformation (Philippot & Kienast, 1989). Type-2 veins are decimetres-thick variably deformed fracture fillings, which consist of omphacite with minor garnet, rutile, apatite and zircon. Type-2 veins tend to randomly cross-cut the mylonitic fabric of the host eclogite. However, formation of both vein types probably involved repeated crack initiation and growth during progressive deformation (Philippot & van Roermund, 1992). The similar mineralogy between the veins and hosting eclogites indicates that the veins formed under eclogite-facies conditions from locally sourced fluids (Philippot, 1987; Philippot & Kienast, 1989; Philippot & van Roermund, 1992). Preservation of fine-scale (centimetres to millimetres) heterogeneities in fluid inclusion and stable isotope compositions (Philippot & Selverstone, 1991; Nadeau *et al.*, 1993) has been cited as evidence for highly restricted fluid movement through these rocks (see also Philippot, 1993). However, Philippot & Kienast (1989) reported for Type-2 veins kosmochlor ($NaCrSi_2O_6$)-rich pyroxene compositions in the cores of some omphacite grains and as inclusions in garnet grains. These Cr-rich grains were interpreted to reflect parental fluids derived from neighbouring Mg–Al metagabbros or talc schists (Philippot & Kienast, 1989). This is an important observation, as it suggests that external fluids also played a role in vein formation.

SAMPLE DESCRIPTION

Samples of veins and adjacent host-rocks were collected from two localities in the Lago Superiore Unit. The first locality is within the Fe–Ti eclogite bodies that crop out along the northwestern side of Lago Superiore [i.e. similar to the sample locality of Cliff *et al.* (1998) and sample locality 3 of Philippot & Kienast (1989)], and the second locality is a large Fe–Ti eclogite body lying midway between Lago Superiore and Lago Chiaretto [i.e. similar to the sample locality of Rubatto & Hermann (2003)]. We have examined in detail two samples of Type-1 dilatational fractures (one from each locality) and several samples of the Type-2 veins and the host eclogite from each locality. Petrographic features of these samples are presented in Table 1. Some of our samples include vein material and surrounding wall-rock (MV5, MV3, MV8), and other samples represent only vein material (MV1, MV4, MV4a, MV6, MVrut) or only host-rock (MV2, MV7). In the field, all veins are completely enclosed within the Fe–Ti eclogite and appear to be isolated from the surrounding Mg–Al metagabbro by at least several metres to tens of metres, whereas serpentinites crop out considerably farther away (some hundreds of metres). However, we stress that this is a qualitative judgement only, as the present outcrop exposure prevents a complete assessment of the extent of veining and the dimension of the eclogite bodies. The following sample descriptions do not distinguish between the two sample localities because we find no significant difference between them. We have also analysed several representative samples of Mg–Al metagabbro and one antigorite serpentinite, which crop out in the surrounding area.

The host metagabbros are fine-grained mylonitic eclogites, which consist largely of omphacite and garnet in roughly equal proportions. Grain sizes rarely exceed 0·5 mm. Garnet may be present as whole, or partial, euhedral crystals (Fig. 1b), but may also form characteristic atoll morphologies (e.g. Philippot & van Roermund, 1989). Inclusions of omphacite, rutile, zircon and apatite are common in garnet. Small (<0·1 mm) grains of rutile

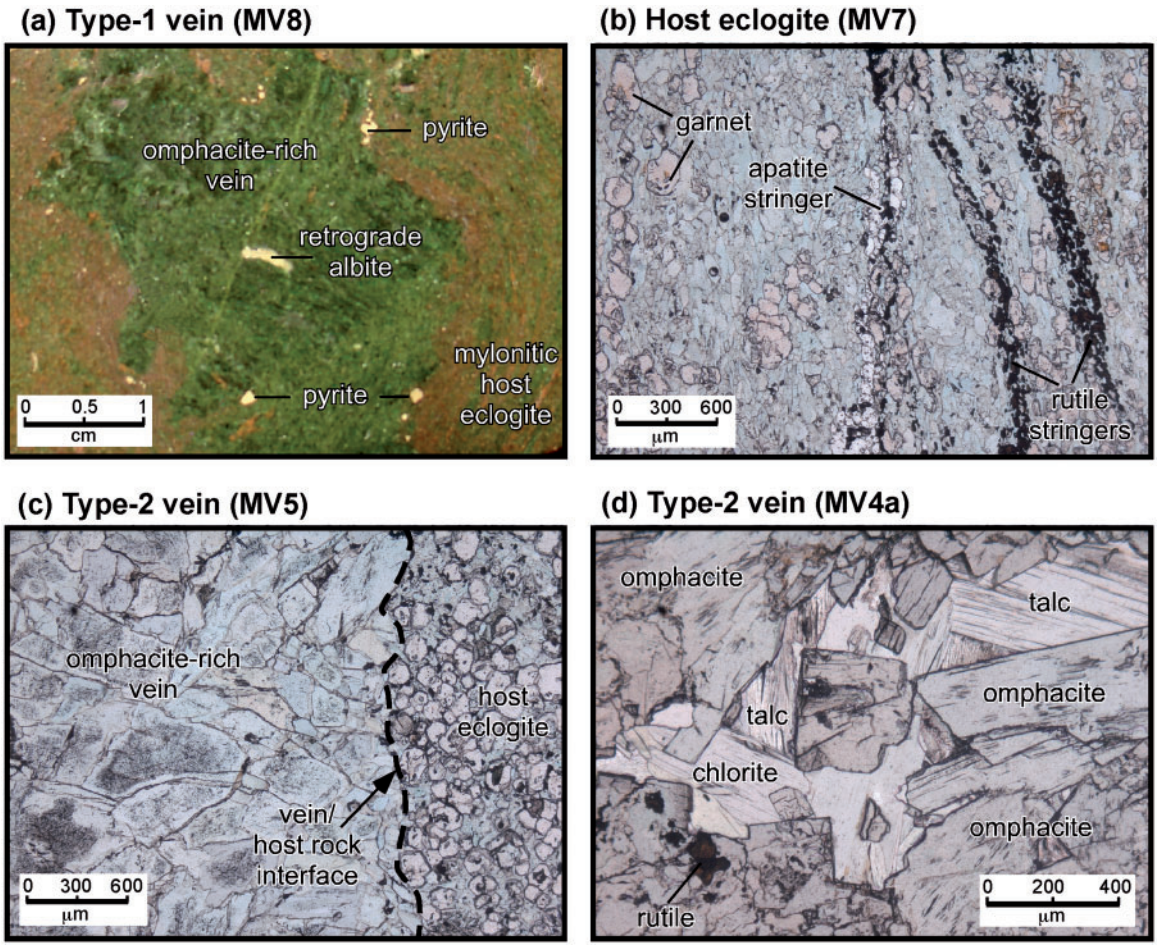

Fig. 1. (a) Photograph of a section across Type-1 vein sample MV8 cutting mylonitized Fe–Ti eclogite. (b) Plane-polarized thin-section photomicrograph of host eclogite sample MV7. (Note the stringers of rutile and apatite that define the foliation.) The two small round spots in the left side of the image are LA-ICP-MS craters. (c) Plane-polarized thin-section photomicrograph of Type-2 vein sample MV5 showing the sharp interface between the vein and the host-rock, and the coarse blocky texture of omphacite in the vein. The dark cores of some omphacite grains are fluid inclusion-rich zones. (d) Plane-polarized thin-section photomicrograph of a chlorite- and talc-rich zone in Type-2 vein sample MV4a. The texture indicates that talc, chlorite and omphacite stably coexist in this case.

and apatite are present in foliation-parallel bands (Fig. 1b). Accessory minerals include quartz, zircon, phengite, blue amphibole, talc and, in some cases, coarse pyrite. Greenschist-facies retrogression is seen as rare interstitial grains of chlorite, albite and epidote, and thin tremolite overgrowths on blue amphibole.

The interface between both vein types and their host metagabbros is sharp and irregular at the sub-millimetre scale (Fig. 1a). The alteration envelopes or selvages found around some veins in other eclogitic terranes (e.g. Spandler & Hermann, 2006; John *et al.*, 2008) are not present around the Monviso veins. The sampled Type-1 dilatational fractures (MV3 and MV8) are lenticular pods up to 2 cm thick and 20 cm long, oriented nearly parallel to the foliation. These veins consist almost entirely of bladed to fibrous omphacite, which may reach 10 mm in length. The omphacite features oscillatory zoning and often has a core zone containing abundant tiny (<10 μm) fluid inclusions. Accessory pyrite is found mainly near contacts between the Type-1 veins and host-rocks (Fig. 1a). Rare clusters of apatite and rutile in the veins are interpreted to be inclusions of host-rock material. Evidence of retrogression in Type-1 veins is limited to rare, fine-grained chlorite and green amphibole laths found along omphacite grain boundaries and rare coarse albite porphyroblasts (Fig. 1a).

Type-2 veins are generally are 5–10 cm thick and 0·5–1 m long, but may be up to 0·5 m thick and several metres long. These veins also have sharp contacts with their host eclogite (Fig. 1c), but tend to cut the eclogite in random orientations, often with anastomosing or branching forms. Type-2 veins appear massive in hand sample, but have heterogeneous internal structures at the thin-section scale. The veins consist largely (>90%) of omphacite grains of variable size and form. Most veins are

Table 1: Description of samples examined in this study

Sample	Rock-type	Description
Western side of Lago Superiore		
MV1	Type-2 vein	Massive vein sample comprising >95% coarse (up to 10 mm) bladed omphacite grains with ~2% garnet (up to 5 mm) and ~1% rutile (up to 0·5 mm). Pyrite is present in trace amounts. Cr-rich omphacite forms ~3% of the sample
MV2	Fe–Ti eclogite	Representative host rock sampled within 1 m of vein samples MV3, MV4 and MV4a. The rock is a fine-grained (0·1–0·5 mm) foliated eclogite with garnet porphyroblasts (~60%) set in a matrix of omphacite grains (~35%). The foliation is defined by garnetiferous bands, up to 10 mm thick, and stringers of rutile grains (2%)
MV3	Type-1 vein and enclosing host rock	The host rock to this vein is similar to sample MV2. The vein consists almost entirely of coarse (up to 7 mm) oscillatory-zoned omphacite grains that lack a preferred orientation. The vein also contains millimetre-sized inclusions of host rock and rare coarse albite grains of retrograde origin
MV4a	Core portion of Type-2 vein	The sample mainly consists of coarse omphacite (~90%) coexisting with lathlike chlorite (~5%) and talc (~5%). Irregular zoning is present in some omphacite grains. Subhedral garnet (up to 1 mm), rutile (>100 μm) and apatite (>100 μm) are accessory phases. Cr-rich omphacite forms ~1% of the sample
MV4	Talc schist selvage to sample MV4a	Strongly foliated schist consisting of coarse talc (~90%) and chlorite (~10%), with minor omphacite and accessory apatite and sulfide that has partly altered to Fe-oxide
Between Lago Superiore and Lago Chiaretto		
MV5	Type-2 vein and enclosing host rock	The host rock is a fine-grained (0·1–0·5 mm) banded eclogite comprising atoll garnet (~50%), omphacite (~50%), and stringers of coarse (up to 0·5 mm) rutile (~2%). The vein lacks a dominant foliation and has sharp and irregular contacts with the host rock. The vein is >95% omphacite of variable size and habit (<0·1 to >5 mm; irregular to bladed) that in some cases shows oscillatory zoning. Cr-rich omphacite forms ~5% of the vein and coarse (up to 2 mm) garnet porphyroblasts; talc and rutile are present as accessory phases (see also Figs 1c and 2)
MV6	Type-2 vein	Coarse-grained foliated vein of >90% bladed omphacite (often zoned) with minor garnet (~5%) and rutile (~1%). Garnet grains tend to form elongate clusters that parallel the foliation. Retrograde chlorite, epidote and albite are present in minor amounts. Cr-rich omphacite forms ~7% of the sample
MV7	Fe–Ti eclogite	Representative host rock sampled within 2 m of vein samples MV5 and MV6. The sample is a fine-grained (0·1–0·5 mm) foliated eclogite with porphyroblastic and atoll garnets (~50%) in a matrix of omphacite grains (~45%). Bands of fine rutile (4%) and apatite (1%) grains define the foliation (see Fig. 1b)
MV8	Type-1 vein and enclosing host rock	The host rock is a equigranular (0·1–0·5 mm) foliated eclogite comprising omphacite (~70%), garnet (~25%), rutile (2%) and accessory apatite, pyrite and blue amphibole. The vein is a 2 cm × 10 cm segregation oriented parallel to the rock foliation, and consists almost entirely of irregular omphacite grains (up to 5 mm) aligned with the foliation. Coarse albite and pyrite grains are present as accessory phases. Inclusions of apatite and rutile stringers derived from the host rock are also present in the vein (see also Fig. 1a)
MVrut	Rutile from Type-2 vein	5 mm × 12 mm rutile crystal extracted from a type 2 vein consisting of oscillatory zoned omphacite, with accessory garnet and talc
Other samples from the Lago Superiore Unit that were analysed for bulk-rock chemical compostion		
MV9 MV-G2F MV-G2C W-86112	Mg–Al eclogite (metagabbro)	Coarse-grained foliated gneisses comprising distinctive green porphyroblasts (up to 5 cm) of zoned Cr-rich omphacite (smaragdite) in a matrix of epidote, garnet, talc, tremolite and Mg-chloritoid. Minor minerals include rutile, white mica, quartz and opaque oxides
W-86124	Serpentinite	Weakly foliated fine-grained serpentinite consisting of >90% antigorite grains that form pseudomorphs after orthopyroxene and the rock matrix. Clusters of fine magnetite form 5–10% of the rock

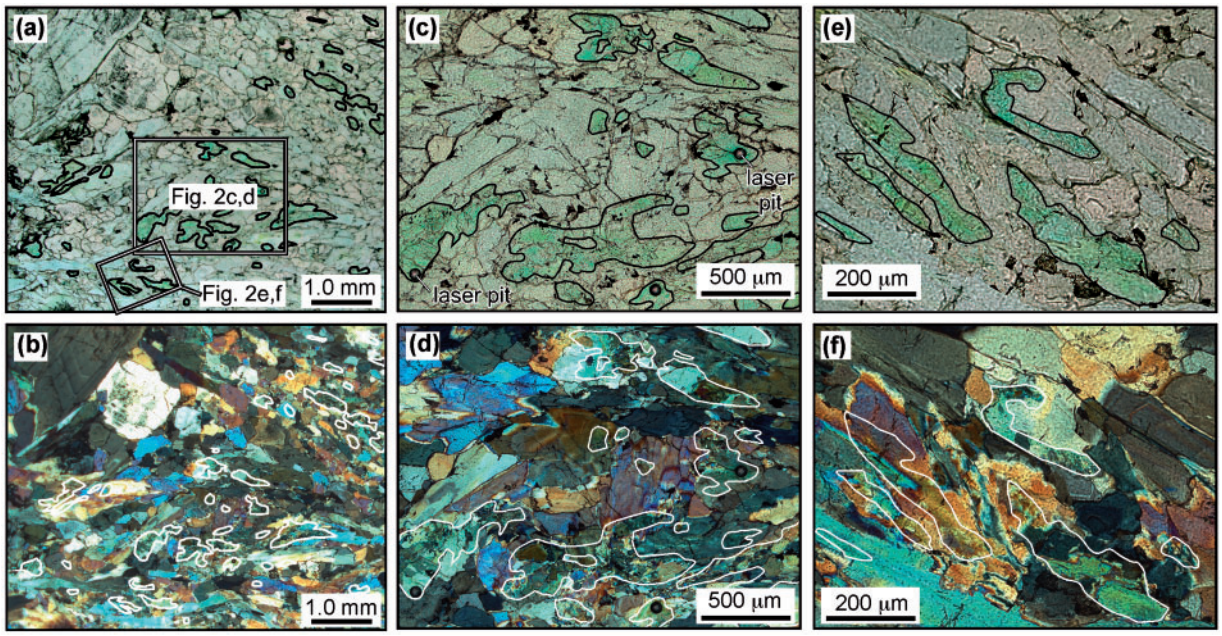

Fig. 2. Thin-section photomicrographs of Cr-rich omphacite domains in Type-2 vein sample MV5. (a), (c) and (e) are under plane-polarized transmitted light (PPL); (b), (d) and (f) are under cross-polarized transmitted light (CPL). The Cr-rich omphacite zones appear green in PPL and are outlined in black in the PPL images and white in the CPL images. It should be noted that the Cr-rich omphacite is not aligned with any single orientation, has irregular textures under CPL and can occupy any part of the original low-Cr omphacite grain. For example, in (c) and (d) Cr-rich omphacite occurs in the core zone of some grains, whereas in (e) and (f) Cr-rich domains clearly forms the rim of one grain.

dominated by aggregates of coarse (0·2–2 mm) blocky to bladed omphacite grains, which often show distinctive oscillatory (see Fig. 2) and, in some cases, sector zoning. This omphacite type tends to have a random orientation, but may be interspersed with foliated domains of finer (<1 mm) omphacite with irregular or stretched morphologies and strained birefringence (Fig. 2). Cutting across both omphacite types are fractures filled with large (up to 20 mm) bladed omphacite crystals aligned perpendicular to, or radiating out from, the fracture walls (see Electronic Appendix 1, which is available for downloading at http://www.petrology.oxfordjournals.org). Overall, these fractures are minor components, which tend to occur close to the margins of the veins.

Some of the Type-2 veins feature a talc-rich margin, up to 10 cm thick and surrounding the omphacite-rich vein core. Talc and sometimes chlorite are also present as minor phases in our Type-2 vein samples (Fig. 1d). There are at least two generations of talc; early talc is in equilibrium with the blocky or bladed omphacite, whereas late talc coexists with greenschist-facies albite and chlorite.

Other minerals found in Type-2 veins are millimetre-scale garnet porphyroblasts (~2% of the veins), which may be dispersed throughout the veins or clustered into thin (<1 cm) stringers, and rare rutile crystals (up to several centimetres long). Vein rutile contains abundant exsolved lamellae of ilmenite. Neither garnet nor rutile is found in the late omphacite-filled fractures. Accessory zircon grains occur in the vein matrix and as micrometre-sized inclusions in garnet and rutile. Apatite was found only as inclusions in garnet. The retrograde overprint of the Type-2 veins resembles that of the Type-1 veins described above.

Philippot & Kienast (1989) reported rare kosmochlor-rich omphacite cores to some Type-2 vein omphacite grains. Kosmochlor-rich omphacite is not readily identifiable in the field or in hand sample, but is easily recognized in thin section by its distinctive deep green colour (Fig. 2). It was found in all the Type-2 vein samples examined, despite forming only <5 vol. % of most samples. The Cr-rich omphacite does not form distinct grains, but occurs as irregular, diffuse zones that may occupy any section of the hosting low-Cr omphacite grains. The Cr-rich zones are usually discordant to the principal zoning structure of the omphacite (see Fig. 2 and Electronic Appendix 1) and are commonly associated with tiny (<5 μm) inclusions of rutile. Cr-rich zones may occur within isolated omphacite grains, may straddle multiple grains (e.g. Electronic Appendix 1), or may form clusters of zones that involve multiple omphacite grains. Cr-rich omphacite is almost exclusively found in the blocky and fine-grained foliated omphacite domains. In rare cases it occupies bladed omphacite and it has not been observed in the late-stage coarse omphacite-filled fractures. Under cross-polarized

light, the Cr-rich omphacite shows an irregular intergrowth-like texture with low-Cr omphacite (Fig. 2) that is interpreted to have formed during fluid-assisted recrystallization of pre-existing omphacite grains. However, structural continuity of Cr-rich zones cannot be traced for more than 10 mm in any sample, so the original flow pathways of fluids forming these zones are not recognized beyond the microscopic scale. These Cr-rich zones in omphacite, and other newly discovered Cr-rich minerals in the Type-2 veins (see below), are the focus of this paper.

ANALYTICAL TECHNIQUES

Bulk-rock geochemical analysis

Twelve fist-sized samples of Type-2 veins, Fe–Ti eclogitic host-rock, serpentinite and Mg–Al metagabbro from the Lago Superiore Unit were crushed in a steel jaw crusher and then milled to a fine powder in a tungsten carbide mill. A small amount of crushed, inclusion-free hydrothermal quartz was milled between each sample to prevent cross-contamination between samples. Loss on ignition (LOI) was calculated by measuring the weight loss from *c.* 2 g of powdered sample after heating to 1050°C for 2 h. Approximately 1·5 g of the devolatilized sample powder was mixed with di-lithium tetraborate ($Li_2B_4O_7$) flux (flux:sample = 5:1) and melted in Pt crucibles using a Claisse M4® fluxer at *c.* 1300°C, and then poured to form homogeneous glass tablets for X-ray fluorescence (XRF) analysis. Major and selected trace element concentrations of the glass tablets were determined using an Axios, PANalytical wavelength-dispersive XRF spectrometer at the Institute of Mineralogy and Petrology, ETH, Zürich, Switzerland.

Comprehensive trace element analysis of the samples was conducted on the fused glass tablets by laser ablation inductively coupled plasma mass spectrometry (LA-ICP-MS) at the Institute of Mineralogy and Geochemistry, University of Lausanne, Switzerland. The instrument consists of an Elan DRC 6100 quadrupole ICP-MS system (Perkin Elmer) coupled to a Geolas 193 nm ArF excimer laser system from Lambda Physik. Ablation was conducted in He–H_2 with laser repetition rates and laser fluence at the sample site set to 10 Hz and ~10 J cm^{-2}, respectively. The ICP-MS system was tuned to ensure robust plasma conditions (e.g. Pettke, 2008), while maximizing signal to background intensity ratio and retaining low oxide production levels (<0·5% ThO). Each fused glass tablet was analysed three times with a 60 μm diameter laser spot and analysis time of ~25 s each. Bracketed external standardization used NIST SRM 612 glass, with element reference values taken from a list of working values compiled from literature sources and interlaboratory testing (see Electronic Appendix 2, which is available for downloading at http://www.petrology.oxfordjournals.org). Internal standardization was achieved using CaO concentrations determined previously by XRF. To evaluate trace element contributions and polyatomic interferences from the $Li_2B_4O_7$ flux, we also prepared and analysed fused discs made from trace-element poor quartz. Measured trace elements were all below detection limits, except for Sc (0·8 ppm), V (1·2 ppm), Cu (0·1 ppm), Zn (2·3 ppm) and Pb (0·025 ppm). Apparent concentrations of Sc and V probably represent Li-argide and B-argide interference, whereas Cu, Zn and Pb may be impurities in the flux. We therefore present XRF data for the transition metals and LA-ICP-MS data for the remaining trace elements. We consider our Pb concentrations not significantly contaminated by flux because the flux Pb concentration is at least five times lower than the lowest concentration of Pb measured in our samples. Flux contributions to the sample Pb values were thus not corrected for.

X-ray mapping and mineral major-element analysis

In situ X-ray mapping of vein minerals and major-element mineral compositions were determined on polished thin sections by wavelength-dispersive spectrometry using a JEOL JXA 8200 superprobe, housed at the Institute of Geological Sciences, University of Bern. Prior to mapping, 3–5 min X-ray line scans were conducted to qualitatively characterize chemical zoning features and X-ray intensities from both host-rock and vein mineral grains. Following these preliminary scans, X-ray mapping of vein omphacite, garnet and rutile was conducted using a beam of 15 kV acceleration voltage and either 40 or 50 nA current. Mapping was completed by scanning the stage in steps of between 1 and 3 μm, with the peak counting time set to between 250 and 450 ms per point. Element maps were collected for Cr, Al, Na, Mg, Ca and Fe in omphacite, Cr, Fe, Mn, Mg and Ca in garnet, and Cr, Al, Fe and Ti in rutile.

Quantitative major element analyses of clinopyroxene, garnet, rutile, talc and antigorite were carried out using a focused beam of 15 kV acceleration voltage and 20 nA beam current. Counting times were 20 s on peak and 20 s on background for each element. The data were processed using φ(ρZ) corrections and standardized against a set of well-characterized, in-house oxide (rutile, ilmenite, eskolaite) and silicate (albite, almandine, forsterite, wollastonite) standards. Fe^{2+} and Fe^{3+} contents of clinopyroxene were calculated on the basis of charge balance, assuming perfect stoichiometry. All Fe was assumed to be Fe^{2+} for the garnet and talc analyses and Fe^{3+} for rutile analyses. These assumptions are supported by the fact that calculated cation totals for these minerals approach ideal stoichiometry. Major element analyses of minerals are presented in Electronic Appendix 3, which is available for downloading at http://www.petrology.oxfordjournals.org.

Mineral trace-element analysis

Vein and host-rock minerals were analysed for trace elements *in situ* on polished thick sections by LA-ICP-MS at the Institute of Geological Sciences, University of Bern, Switzerland, using an Elan DRC-e quadrupole ICP-MS system coupled to a Geolas Pro 2006 193 nm ArF excimer laser system from Lambda Physik. Laser energy was regulated using an inline attenuator to provide a laser fluence at the sample site of 10–15 J cm^{-2}. Ablation was conducted in a custom-built sample chamber and a He–H_2 mixture (1000:7 ratio) was used as the aerosol transport gas. Plasma operational protocols were similar to those listed above for the bulk-rock trace element analyses. Analysis of minerals was conducted using 8–10 Hz repetition rate and beam diameters of 44–60 μm for clinopyroxene, rutile, talc, antigorite and zircon, and 44–90 μm for garnet. All analyses were conducted using a fixed beam position, except for one traverse across a large vein rutile crystal that was obtained by scanning a 44 μm beam across the width of the crystal at a rate of *c.* 8 μm s^{-1}. Each signal was carefully evaluated during off-line data reduction, and integration intervals were set to avoid contributions from accidentally ablated inclusions and/or cracks. Isotopes used for internal standardization were ^{43}Ca for clinopyroxene and garnet, ^{49}Ti for rutile, ^{25}Mg for talc and ^{29}Si for zircon and antigorite. External standardization was carried out using NIST SRM 612 glass, which was analysed using a beam diameter of 44 μm and repetition rate of 10 Hz. Standard reference values are presented in Electronic Appendix 2 (which is available for downloading at http://www.petrology.oxfordjournals.org). The analytical conditions minimized mass-load dependent element fractionations (e.g. Kroslakova & Gunter, 2007). None the less, early testing of our analytical protocols revealed anomalous behaviour for some elements, particularly Sb and As, during analysis. In Electronic Appendix 2, we describe these problems and the additional procedures that were employed during data acquisition to achieve accurate measurements of all analyzed elements. Trace element data of minerals are presented in Electronic Appendix 4, which is available for downloading at http://www.petrology.oxfordjournals.org.

In situ Hf isotope measurements of zircon

Zircon grain separates from an eclogitic host-rock and Type-2 vein studied by Rubatto & Hermann (2003) were chosen for Hf isotope analysis. These samples were collected from our second sampling locality. Cathodoluminescence was used to image internal zoning of zircon grains to guide isotopic analysis. Instrumental set-up for Hf isotopic analysis follows that of Hiess *et al.* (2009). Analysis was completed using a custom-made 'HelEx' laser ablation system with a 193 nm ArF laser coupled to a Thermo-Finnigan Neptune multicollector (MC)-ICP-MS system at the Australian National University, Canberra. Ablation was conducted in a He atmosphere, with Ar and N_2 introduced after the ablation cell with the intent to suppress surface deposition (Eggins *et al.*, 1998) and increase sensitivity (Durrant, 1994), respectively. Laser operating conditions were 5 Hz and 50 mJ. Data were collected through 120 cycles over a period of *c.* 2 min with a spot size of 47 μm. Baseline measurements were acquired on peak with a shutter blocking the laser. To correct for systematic instrument bias (Wang *et al.*, 2009), we normalized the $^{176}Hf/^{177}Hf$ measurements to the values of the Mud Tank zircon standard. Data were processed off-line using a spreadsheet to correct for amplifier response factors, baseline, isobaric interference and mass bias. Yb and Hf mass bias factors were measured during each analysis, but for the Yb-poor zircon of the vein, mass bias could not be measured accurately for Yb. For such analyses, Yb mass bias correction was based on the measured Hf mass bias and the ratio of Yb/Hf mass bias factors of the day. Isobaric interferences are ^{176}Yb and ^{176}Lu on ^{176}Hf, which are corrected for by measuring ^{173}Yb and ^{175}Lu and adopting the $^{173}Yb/^{171}Yb$, $^{176}Yb/^{173}Yb$ and $^{176}Lu/^{175}Lu$ of Thirlwall & Anczkiewicz (2004). CHUR values of $^{176}Lu/^{177}Hf = 0{\cdot}0332$ and $^{176}Hf/^{177}Hf = 0{\cdot}282772$ (Blichert-Toft & Albarède, 1997) and a ^{176}Lu decay constant of $1{\cdot}867 \times 10^{-5}$ Ma^{-1} (Söderlund *et al.*, 2004) were adopted.

BULK-ROCK GEOCHEMISTRY

The vein-hosting Fe–Ti eclogites (Table 2) have mafic compositions with high Fe_2O_3 and TiO_2, but low Cr (7·5–55 ppm) and Ni (32–46 ppm) contents relative to mid-ocean ridge basalt (MORB) (Sun & McDonough, 1989). These compositions are comparable with other Lago Superiore eclogites analysed by Schwartz *et al.* (2000) and Hermann & Rubatto (2003) and are similar to fractionated ferrobasalts of the oceanic crust (e.g. Carmichael, 1964; Wood, 1978). However, some element concentrations [e.g. Na_2O, Sr, light rare earth elements (LREE)] vary significantly between the eclogite samples. The Mg–Al metagabbro samples also have mafic compositions, but are richer in MgO, Al_2O_3, CaO, Cr, Ni (Fig. 3) and Sr compared with the Fe–Ti eclogites (or MORB; Sun & McDonough, 1989). The Mg–Al metagabbros have low contents of most incompatible elements, but all samples feature positive Eu anomalies (Table 2). These chemical characteristics are consistent with a plagioclase-rich cumulate protolith. We analysed one serpentinite, and our data are consistent with the Monviso serpentinite data of Hattori & Guillot (2007). The serpentinite has a composition typical of hydrated mantle rock (e.g. high LOI, MgO, Cr and Ni) but also has high As and Sb contents (Table 2) relative to typical mantle peridotite.

The bulk major element composition of the Type-2 veins reflects their high modal abundances of omphacite and, in

Table 2: Bulk-rock composition of Lago Superiore samples

Sample:	MV2	MV7	MV8	MV1	MV6	MV4 A	MV4	MV9	W-86112	MV-G2F	MV-G2C	W-86124
Rock type:	Fe–Ti ecl	Fe–Ti ecl	Fe–Ti ecl	T2 vein	T2 vein	T2 vein	T2 vein	Mg–Al ecl	Mg–Al ecl	Mg–Al ecl	Mg–Al ecl	serp
Major element oxides (XRF) (wt %)												
SiO_2	43·2	44·2	49·6	54·7	54·1	48·8	53·0	50·0	50·1	47·3	49·1	39·3
TiO_2	2·35	4·73	2·26	0·14	0·16	0·11	0·18	0·27	0·25	0·18	0·25	0·022
Al_2O_3	15·4	12·7	13·8	9·43	8·94	6·92	3·78	17·5	16·5	19·8	16·3	1·35
Fe_2O_3	19·9	17·2	12·9	7·28	9·20	7·53	7·74	3·39	4·65	4·89	4·23	8·74
MnO	0·53	0·23	0·18	0·04	0·05	0·06	0·05	0·05	0·09	0·09	0·07	0·082
MgO	7·11	5·02	5·41	7·92	7·43	16·4	27·6	9·12	10·6	9·7	11·2	37·6
CaO	9·50	10·9	9·35	11·9	11·2	13·9	0·40	13·6	12·7	12·6	12·5	0·004
Na_2O	2·28	4·07	6·15	7·51	7·33	2·88	<0·009	2·85	2·42	1·47	2·72	<0·01
K_2O	0·009	0·019	0·037	0·011	0·011	0·014	0·005	0·027	0·021	0·013	0·016	0·004
P_2O_5	0·10	0·69	0·19	0·011	0·018	0·48	0·08	0·009	0·017	0·015	0·03	0·005
Cr_2O_3	0·006	<0·001	0·007	0·16	0·24	0·17	0·340	0·16	0·22	0·10	0·35	0·38
NiO	0·004	0·002	0·005	0·035	0·017	0·07	0·23	0·022	0·031	0·033	0·035	0·29
LOI	n.d.	n.d.	n.d.	0·11	0·11	2·92	5·97	2·53	2·90	3·69	3·06	11·6
Total	100·4	99·8	99·9	99·2	98·8	100·3	99·4	99·5	100·5	99·9	99·9	99·4
Trace elements (XRF) (ppm)												
Sc	45	41	32	18	23	31	7	39	32	17	36	10
V	365	485	372	296	359	315	71	124	111	55	114	55
Cu	21	13	117	33	22	24	14	36	135	40	45	21
Zn	43	75	79	79	127	106	186	29	34	31	32	51
Ga	9	21	20	26	24	14	11	13	12	12	6	2
Trace elements (LA-ICP-MS) (ppm)												
Sc	43	41	33	15	21	30	9	33	31	14	34	13
V	379	481	369	323	372	334	72	129	119	68	124	65
Cr	55	7·5	55	1180	1700	1250	2280	1140	1560	737	2540	2890
Co	332	271	134	84	58	83	69	64	68	66	44	106
Ni	43	32	46	271	124	553	1570	166	230	251	263	2270
As	<0·12	<0·21	<0·20	<0·13	<0·14	<0·15	<0·12	<0·15	<0·14	<0·15	<0·15	1·42
Rb	0·27	0·57	0·83	0·28	0·38	0·29	0·04	0·40	0·39	0·16	0·25	0·035
Sr	26	80	220	44	39	89	4·56	162	154	243	162	0·24
Y	63	60	31	4·93	4·69	17·1	2·13	6·41	6·04	4·86	5·88	2·97
Zr	65	120	108	23·4	53	14·8	12·9	8·11	8·88	7·11	11·2	0·25
Nb	2·80	6·11	2·38	0·32	0·28	0·78	0·10	0·20	0·23	0·22	0·18	0·060
Sb	<0·05	<0·07	<0·08	<0·06	<0·06	<0·07	<0·05	<0·07	<0·06	<0·06	<0·06	0·063
Cs	0·023	<0·018	0·051	0·026	0·052	0·019	<0·017	<0·027	0·041	<0·017	<0·027	<0·014
Ba	0·87	1·13	4·06	1·25	2·68	1·88	0·32	3·69	1·71	2·41	2·64	0·49
La	0·98	9·1	5·33	0·50	0·48	6·17	0·92	0·43	0·56	0·62	0·48	0·34
Ce	3·72	31	18·2	1·92	1·90	22·7	2·91	1·53	1·68	2·02	1·57	1·19
Pr	0·69	5·38	3·15	0·40	0·37	4·07	0·51	0·28	0·30	0·33	0·30	0·21
Nd	4·58	29·0	17·3	2·67	2·38	25·0	2·68	1·63	1·50	1·59	1·68	0·99
Sm	3·27	8·56	5·77	1·59	1·36	8·71	0·79	0·72	0·62	0·56	0·66	0·29
Eu	2·46	2·82	2·44	0·62	0·54	2·52	0·24	0·40	0·40	0·43	0·36	0·09
Gd	11·6	9·90	6·18	2·02	1·66	6·76	0·69	1·04	0·87	0·82	0·87	0·38
Tb	1·80	1·56	0·83	0·24	0·20	0·58	0·08	0·17	0·15	0·15	0·17	0·07
Dy	11·8	10·7	5·64	1·18	1·16	3·25	0·43	1·16	1·13	0·93	1·05	0·46

(continued)

Table 2: Continued

Sample:	MV2	MV7	MV8	MV1	MV6	MV4 A	MV4	MV9	W-86112	MV-G2F	MV-G2C	W-86124
Rock type:	Fe–Ti ecl	Fe–Ti ecl	Fe–Ti ecl	T2 vein	T2 vein	T2 vein	T2 vein	Mg–Al ecl	Mg–Al ecl	Mg–Al ecl	Mg–Al ecl	serp
Er	6·29	6·56	3·29	0·54	0·40	1·96	0·27	0·57	0·71	0·46	0·62	0·36
Yb	5·47	5·50	2·79	0·30	0·35	2·03	0·20	0·54	0·52	0·44	0·63	0·30
Lu	0·77	0·78	0·45	0·06	0·04	0·33	0·03	0·09	0·09	0·06	0·09	0·06
Hf	1·64	2·85	2·49	0·56	1·24	0·40	0·34	0·24	0·32	0·18	0·33	0·03
Ta	4·82	4·46	1·79	1·18	1·02	0·69	0·015	0·84	0·70	0·73	0·30	0·08
Pb	0·63	0·28	0·65	0·18	0·24	0·44	0·16	0·19	0·14	0·36	0·23	0·31
Th	0·046	0·12	0·09	0·046	0·036	0·11	0·025	0·014	0·030	0·013	0·017	0·009
U	0·027	0·053	0·040	0·029	0·013	0·018	0·013	0·015	0·019	0·015	0·006	0·018
Eu*	1·09	0·93	1·24	1·05	1·08	0·96	0·96	1·42	1·66	1·95	1·45	0·83

Rock-types: ecl, eclogite; T2, Type-2; serp, serpentinite. n.d., not detectable; LOI, loss on ignition; Eu* represents the Eu anomaly calculated using the formula $Eu^* = Eu_N/[0{\cdot}5(Sm_N + Gd_N)]$, where N refers to the chondrite normalized value taken from Taylor & McLennan (1985).

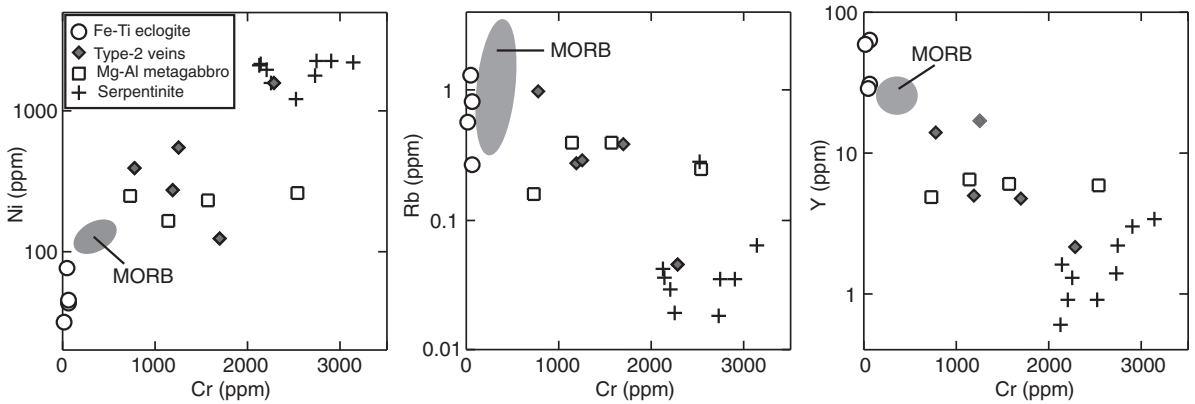

Fig. 3. Variation of bulk-rock Cr vs Ni, Rb, and Y for the Monviso rock-types, Type-2 veins and MORB. Data for Monviso are taken from this study (Table 2) and from Rubatto & Hermann (2003) and Hattori & Guillot (2007); MORB data are from Kelemen *et al.* (2003) and Klein (2003). It should be noted that the Type-2 veins have high Cr and Ni and lower Y contents than their host eclogites.

the case of samples MV4 and MV4a, talc. The veins tend to have lower trace element contents than their host-rocks (Table 2: see also Rubatto & Hermann, 2003), although all of the veins are distinctly enriched in Cr and Ni (Fig. 3). Talc-rich sample MV4 has the highest MgO (27·6 wt %), Cr (2280 ppm) and Ni (1570 ppm) contents.

MINERAL MAJOR ELEMENT CHEMISTRY

Eclogitic host-rocks and Type-1 veins

Representative major element compositions for clinopyroxene, garnet, and rutile are presented in Tables 3, 4, and 5, respectively. The full set of major element data of minerals is presented in Electronic Appendix 3, which is available for downloading at http://www.petrology.oxfordjournals.org. Eclogite clinopyroxene is omphacitic, with 34–56 mol % jadeite, 34–52 mol % diopside and 5–15 mol % aegirine components (Table 3). Variations within this compositional range exist on the millimetre scale, possibly reflecting the pre-metamorphic heterogeneity of the rocks. Omphacite Cr_2O_3 and TiO_2 contents are less than 0·08 and 0·1 wt %, respectively. Host-rock garnet is almandine-rich (50–70 mol %) with minor pyrope and grossular contents (Table 4). Spessartine is less than 3 mol %. Many large garnet porphyroblasts preserve major-element zoning, with a grossular-rich (up to 35 mol %) core zone, enclosed by a relatively grossular-poor, and pyrope-, almandine- and spessartine-rich rim. TiO_2 contents are <0·2 wt %, but are higher in garnet cores than rims. Atoll and other

Table 3: Representative major-element analyses (wt %) of omphacite from the host eclogites, Type-1 veins and Type-2 veins

Rock-type:	host	host	host	host	Type-1	Type-1	Type-1	Type-2	Type-2	Type-2	Type-2	Type-2	Type-2	Type-2	Type-2	Type-2	Type-2	Type-2	Type-2
Sample no.:	MV8	MV8	MV3	MV7	MV3	MV3	MV8	MV4a	MV4a	MV4a	MV6	MV6	MV6	MV6	MV5	MV5	MV5	MV1	MV1	MV1
SiO_2	56·8	56·7	56·5	56·2	56·5	56·4	56·3	56·3	55·7	56·1	55·5	55·7	55·6	56·3	56·3	56·2	56·1	56·8	56·8	56·8
TiO_2	0·047	0·062	0·027	0·021	0·052	0·071	0·047	0·025	0·026	0·010	0·028	0·018	0·028	0·029	0·022	0·011	0·011	0·074	0·045	0·061
Al_2O_3	11·4	9·99	9·08	7·64	8·50	8·22	9·77	6·15	4·36	3·72	6·47	8·40	7·39	8·94	10·6	9·05	7·45	9·81	8·91	8·79
Cr_2O_3	0·01	0·063	0·01	<0·01	0·016	0·042	0·02	4·94	2·94	<0·01	3·09	4·24	0·034	0·007	5·89	0·025	1·70	0·023	0·205	0·016
FeO	6·52	7·28	6·80	7·57	5·31	6·72	8·11	4·66	4·70	5·54	6·40	7·41	8·97	7·98	4·63	5·14	5·57	6·24	6·44	6·56
MnO	<0·01	<0·01	0·016	<0·01	0·01	0·049	0·128	<0·01	0·021	0·031	0·052	0·047	<0·01	<0·01	<0·01	0·019	<0·01	0·027	0·074	0·068
MgO	6·46	6·85	7·47	8·15	8·83	8·24	6·62	8·10	10·8	12·5	8·20	5·84	7·78	6·99	4·73	8·82	9·06	7·29	7·80	8·04
CaO	9·93	10·8	11·7	12·5	13·2	12·7	10·6	12·4	16·0	18·5	12·5	8·95	11·9	11·1	7·25	13·1	13·2	11·4	11·7	12·2
Na_2O	8·76	8·23	7·83	7·22	6·87	7·22	8·39	7·56	5·33	3·99	7·14	9·09	7·54	8·10	9·76	6·86	6·72	8·01	7·78	7·28
Total	99·9	100·0	99·4	99·3	99·3	99·7	100·0	100·1	99·9	100·4	99·4	99·7	99·2	99·4	99·2	99·2	99·8	99·7	99·8	99·8
Atomic formula (calculated to 4 total cations)																				
Si	2·01	2·02	2·02	2·03	2·02	2·02	2·01	2·02	2·01	2·02	2·01	2·00	2·01	2·02	2·03	2·01	2·01	2·02	2·03	2·03
Ti	0·001	0·002	0·001	0·001	0·001	0·002	0·001	0·001	0·001	0·000	0·001	0·000	0·001	0·001	0·001	0·000	0·000	0·002	0·001	0·002
Al	0·47	0·42	0·38	0·32	0·36	0·35	0·41	0·26	0·19	0·16	0·28	0·36	0·31	0·38	0·45	0·38	0·32	0·41	0·37	0·37
Cr	0·000	0·002	0·000	0·000	0·000	0·001	0·001	0·14	0·084	0·000	0·088	0·12	0·001	0·000	0·17	0·001	0·048	0·001	0·006	0·000
Fe^{3+}	0·10	0·11	0·11	0·13	0·07	0·11	0·15	0·08	0·08	0·08	0·12	0·15	0·20	0·15	0·01	0·06	0·08	0·09	0·10	0·07
Fe^{2+}	0·09	0·11	0·09	0·10	0·09	0·09	0·09	0·06	0·07	0·08	0·08	0·08	0·07	0·09	0·13	0·09	0·09	0·10	0·09	0·12
Mn	0·00	0·00	0·00	0·00	0·00	0·001	0·004	0·00	0·001	0·001	0·002	0·001	0·00	0·00	0·00	0·001	0·00	0·001	0·002	0·002
Mg	0·34	0·36	0·40	0·44	0·47	0·44	0·35	0·43	0·58	0·67	0·44	0·31	0·42	0·37	0·25	0·47	0·48	0·39	0·41	0·43
Ca	0·38	0·41	0·45	0·48	0·51	0·49	0·41	0·48	0·62	0·71	0·49	0·35	0·46	0·43	0·28	0·50	0·51	0·44	0·45	0·47
Na	0·60	0·57	0·54	0·50	0·48	0·50	0·58	0·53	0·37	0·28	0·50	0·63	0·53	0·56	0·68	0·48	0·47	0·55	0·54	0·50
Jadeite	51·6	46·9	43·4	38·2	41·8	39·3	43·5	30·0	21·5	19·7	30·5	38·2	33·6	42·2	53·2	42·3	35·3	46·8	43·8	44·5
Diopside	37·7	41·2	44·7	48·1	50·6	48·7	40·5	47·7	62·0	71·1	48·5	34·5	46·1	42·6	28·0	50·1	50·6	43·5	44·5	46·8
Aegirine	9·9	10·9	11·4	13·0	6·7	11·3	15·3	8·4	7·7	8·4	11·5	14·5	19·7	14·7	1·0	6·4	7·9	9·2	10·3	7·3
Kosmochlor	<0·1	0·18	<0·1	<0·1	<0·1	0·12	<0·1	14·0	8·40	<0·1	8·85	12·1	0·10	<0·1	16·8	<0·1	4·82	<0·1	0·58	<0·1

Ferric and ferrous iron was calculated on the basis of charge balance.

Table 4: Representative major-element analyses (wt %) of garnet from the host eclogites and Type-2 veins

Rock-type:	host	host	host	host	host	host	Type-2	Type-2	Type-2	Type-2	Type-2	Type-2	Type-2	Type-2	Type-2
Sample no.:	MV7	MV7	MV7	MV5	MV5	MV3	MV1	MV1	MV5	MV5	MV6	MV6	MV6	MV4a	MV4a
Domain:	core	rim	attol	core	rim	rim	Cr poor	Cr rich	Cr poor	Cr rich	Cr rich	Cr poor	Cr rich	Cr rich	Cr poor
SiO_2	38·1	38·4	38·5	39·1	38·6	38·5	38·6	39·3	39·0	38·5	38·1	38·6	38·0	39·0	38·8
TiO_2	0·053	0·018	0·008	0·018	0·02	0·245	0·083	0·071	0·022	0·051	0·141	0·099	0·108	0·030	0·063
Al_2O_3	20·1	21·0	21·1	21·6	21·3	21·4	21·4	21·2	21·7	20·9	19·1	20·9	17·3	21·2	21·7
Cr_2O_3	0·007	0·002	0·022	0·015	0·032	0·008	0·028	0·129	0·017	0·599	2·11	0·031	4·39	0·727	0·018
FeO	28·6	30·5	30·5	26·9	28·4	29·0	28·4	26·8	27·2	27·7	30·3	31·7	30·5	28·3	25·9
MnO	0·13	0·66	0·60	0·75	1·08	1·01	0·79	1·26	0·51	0·55	0·78	0·61	0·75	0·66	0·56
MgO	1·27	3·24	3·50	6·55	6·18	5·01	6·35	6·14	7·00	5·83	4·70	4·52	4·27	6·75	7·52
CaO	11·83	6·44	6·52	5·81	4·77	5·24	4·67	5·85	4·93	6·06	5·36	4·51	5·27	4·17	5·14
Na_2O	0·02	0·01	0·02	0·03	0·04	0·04	0·02	0·03	0·02	0·03	0·03	0·04	0·02	0·04	0·00
Total	100·1	100·3	100·8	100·8	100·4	100·5	100·3	100·8	100·4	100·2	100·6	101·0	100·6	100·9	99·7
Atomic formula (calculated to 8 total cations)															
Si	3·03	3·03	3·03	3·02	3·00	3·01	3·00	3·03	3·01	3·01	3·01	3·03	3·04	3·01	3·00
Ti	0·003	0·001	0·000	0·001	0·001	0·014	0·005	0·004	0·001	0·003	0·008	0·006	0·007	0·002	0·004
Al	1·88	1·95	1·95	1·96	1·95	1·97	1·96	1·93	1·98	1·92	1·78	1·93	1·63	1·93	1·98
Cr	0·000	0·000	0·001	0·001	0·002	0·001	0·002	0·008	0·001	0·037	0·132	0·002	0·277	0·045	0·001
Fe^{3+}	0·05	0·00	0·00	0·01	0·05	0·01	0·03	0·00	0·00	0·04	0·07	0·02	0·03	0·00	0·01
Fe^{2+}	1·86	2·05	2·02	1·72	1·80	1·89	1·82	1·75	1·76	1·77	1·93	2·06	2·01	1·83	1·67
Mn	0·01	0·04	0·04	0·05	0·07	0·07	0·05	0·08	0·03	0·04	0·05	0·04	0·05	0·04	0·04
Mg	0·15	0·38	0·41	0·75	0·72	0·59	0·74	0·71	0·81	0·68	0·55	0·53	0·51	0·78	0·87
Ca	1·01	0·54	0·55	0·48	0·40	0·44	0·39	0·48	0·41	0·51	0·45	0·38	0·45	0·35	0·43
Na	0·00	0·00	0·00	0·00	0·01	0·01	0·00	0·00	0·00	0·00	0·01	0·01	0·00	0·01	0·00
Spessartine	0·3	1·5	1·3	1·6	2·4	2·2	1·7	2·7	1·1	1·2	1·7	1·3	1·7	1·4	1·2
Almandine	62·0	67·5	66·8	57·5	60·9	63·5	61·1	57·6	58·5	59·7	65·4	68·7	66·9	61·1	55·8
Pyrope	4·9	12·8	13·6	25·0	23·6	19·6	24·3	23·6	26·8	22·4	18·1	17·5	16·7	26·0	28·8
Grossular	32·8	18·3	18·2	15·9	13·0	14·7	12·8	15·7	13·5	14·9	8·2	12·4	0·9	9·3	14·1
Uvarovite	0·02	0·01	0·07	0·04	0·10	0·03	0·09	0·39	0·05	1·85	6·59	0·10	13·9	2·23	0·05

Ferric and ferrous iron was calculated on the basis of charge balance.

small garnet grains are similar in composition to the rims of the large zoned garnet grains. The Cr_2O_3 contents of host-rock garnet and rutile are below 0·05 and 0·03 wt %, respectively.

Clinopyroxene in Type-1 veins shows zoning of ~10 mol % variations in jadeite–diopside–aegerine components. Overall, Type-1 vein omphacite is similar in composition to omphacite of the adjacent host-rock, although the vein omphacite ranges to higher diopside and aegirine contents than the host-rock omphacite (Table 3).

Type-2 veins

Most (>95%) of the omphacite in Type-2 veins contains little Cr (Cr_2O_3 <0·2 wt %) and is similar in composition to omphacite in the host-rocks and Type-1 veins. However, omphacite in Type-2 veins extends to higher diopside contents (Table 3, Fig. 4a) than that from the other rock types.

As observed in thin section, Cr-rich omphacite is only a minor component of Type-2 veins. The Cr_2O_3 content of these Cr-rich domains may reach >6·5 wt %, which corresponds to kosmochlor contents approaching 20 mol %. X-ray mapping and quantitative point analyses of Cr-rich domains reveal no simple relationship between the kosmochlor content and any other major component of the omphacite (Fig. 4). That said, a general trend of decreasing aegirine content with increasing kosmochlor is seen in samples MV4a (Fig. 4b). Sample MV4a omphacite is also relatively rich in the diopside component. X-ray mapping reveals that Cr-rich domains may be confined to a single zone of a crystal, may crosscut major zoning features, or may even traverse clinopyroxene grain boundaries (Electronic Appendix 1).

Type-2 vein garnet is pyrope rich (up to 30 mol %) in comparison with the host-rock garnet (Fig. 5). As with

Table 5: Representative major-element analyses (wt %) of rutile from the host eclogites and Type-2 veins

Rock-type:	host	host	host	Type-2	Type-2	Type-2	Type-2	Type-2	Type-2	Type-2
Sample no.:	MV7	MV7	MV7	MV5	MV5	MV5	MV6	MV6	MV6	MV6
TiO_2	99·7	99·8	99·3	98·6	97·6	99·5	100·0	99·4	97·7	98·0
Al_2O_3	<0·02	0·03	<0·02	0·02	0·02	<0·02	<0·02	0·07	<0·02	<0·02
Cr_2O_3	0·01	0·01	0·03	0·77	0·06	0·05	0·05	0·28	1·41	2·42
Fe_2O_3	0·47	0·73	0·75	0·71	2·82	0·92	0·67	0·41	0·45	0·40
CaO	0·06	0·15	0·19	0·12	0·06	0·07	0·02	0·06	0·35	0·19
Total	100·2	100·7	100·3	100·2	100·6	100·5	100·7	100·2	99·9	101·0
Atomic formula (calculated to 2 oxygens)										
Ti	0·996	0·993	0·993	0·987	0·978	0·992	0·994	0·993	0·983	0·977
Al	0·000	0·000	0·000	0·000	0·000	0·000	0·000	0·001	0·000	0·000
Cr	0·000	0·000	0·000	0·008	0·001	0·001	0·000	0·003	0·015	0·025
Fe	0·005	0·007	0·007	0·007	0·028	0·009	0·007	0·004	0·005	0·004
Ca	0·001	0·002	0·003	0·002	0·001	0·001	0·000	0·001	0·005	0·003
Cation total	1·002	1·002	1·003	1·004	1·008	1·003	1·001	1·002	1·008	1·009

All Fe assumed to be Fe^{3+}.

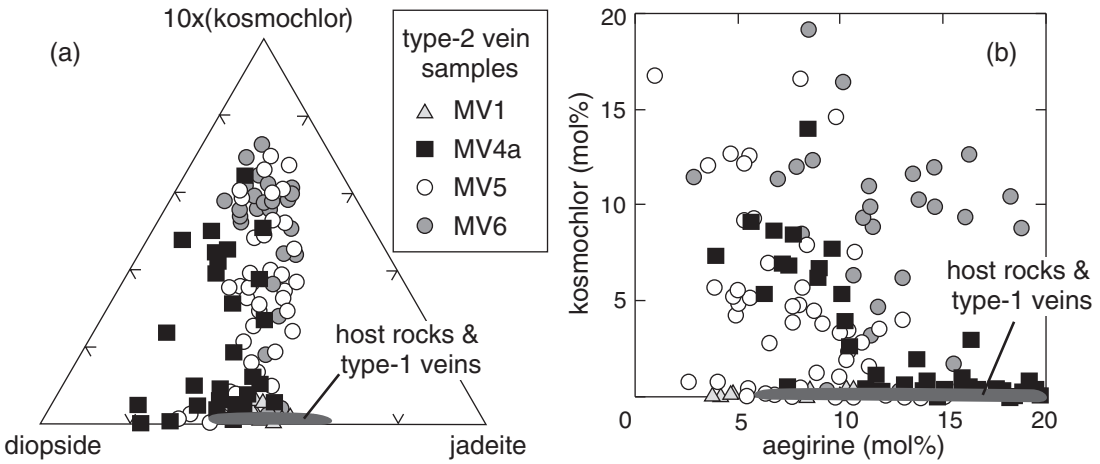

Fig. 4. Major element composition of vein and host-rock omphacite. (a) Diopside, jadeite and kosmochlor components of omphacite plotted in a ternary diagram. It should be noted that the kosmochlor component has been accentuated by a factor of 10. (b) Kosmochlor vs aegirine components of omphacite. Omphacite from Type-2 vein samples MV4a and, to some extent, MV5 show a broad negative correlation between kosmochlor and aegirine components, consistent with substitution of Fe^{3+} for Cr^{3+}. Omphacite major element data are reported in Electronic Appendix 3.

omphacite, Cr shows complex zoning patterns in some garnet crystals (X-ray maps of grains with high-Cr zones are presented in Fig. 6 and Electronic Appendix 1). Chromium contents of the host-rock garnet and Cr-poor domains of the Type-2 vein garnet are similar, whereas Cr-rich vein garnet may contain up to 5 wt % Cr_2O_3. This Cr-rich garnet also tends to be relatively almandine rich (Fig. 5a). The range of TiO_2 contents in vein and host-rock garnet is also similar, although there is a general correlation between the Cr_2O_3 and TiO_2 contents of the vein garnet (Table 4).

Element abundance X-ray maps reveal complex structures within the garnet grains. In some Type-2 vein samples (MV1, MV5, MVrut) the garnet crystals have concentric, oscillatory zoning of Fe, Mn, Ca, Mg and Cr. Several Cr-rich zones may be present in a single grain (Fig. 6a), although there is again no clear relationship between Cr and any of the major elements. Type-2 vein

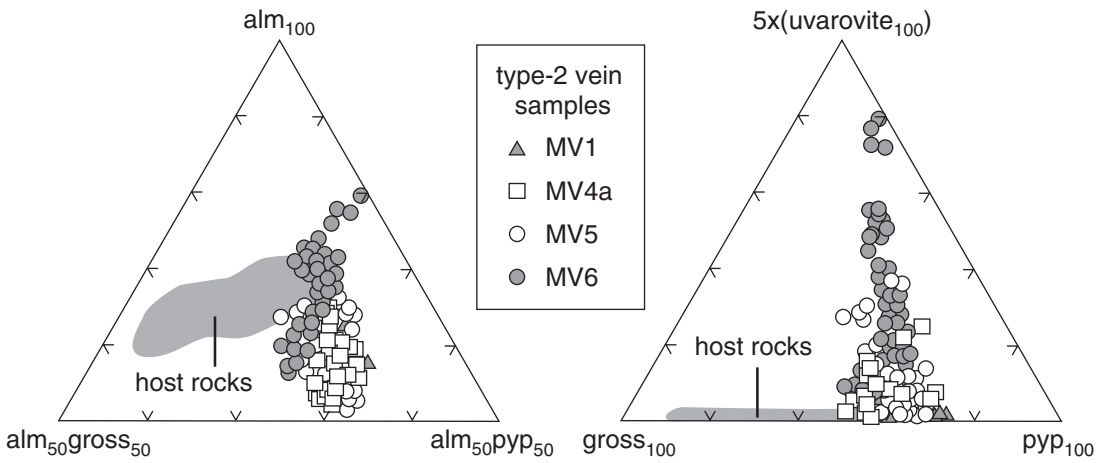

Fig. 5. Ternary plots of major components in Type-2 vein and host-rock garnet. Type-2 vein garnet tends towards higher pyrope and uvarovite ($Ca_3Cr_2Si_3O_{12}$) components compared with the host-rock garnet. Garnet major element data are given in Electronic Appendix 3.

samples (MV6, MV4a and, to some extent, MV5) contain garnet with very complex fracture-like textures that appear to be most pronounced for Cr (see Fig. 6b). There tends to be a dominant orientation to the fracture-like texture of each grain, but the orientation direction varies from grain to grain. The Cr-rich zones also are rich in Ca and poor in Mg compared with Cr-poor garnet, which indicates that Cr substitutes into these garnet crystals as an uvarovite ($Ca_3Cr_2Si_3O_{12}$) component. Many of these garnet grains also have a thin (<50 μm) outer rim zone rich in Ca and Mg and poor in Cr, Fe and Mn (Fig. 6b).

Like garnet, rutile grains in Type-2 veins also have complex zoning structures with Cr-rich zones. Cr_2O_3 contents may reach over 2 wt % in Type-2 vein rutile (Table 5). The Type-2 vein samples that contain concentric oscillatory zoned garnet (MV1, MV5, MVrut) contain rutile grains with complex oscillatory zoning, which is most prominent in Cr (Fig. 7). On the other hand, vein samples that contain fracture-like textured garnet (MV4a and MV6) contain rutile with irregular bands and zones rich in Cr (Fig. 8). Talc coexisting with omphacite in Type-2 veins is Fe poor (Mg-number 90–94), but contains up to 0·4 wt % NiO (Electronic Appendix 3).

MINERAL TRACE ELEMENT CHEMISTRY

Type-1 veins

Type-1 vein (MV3 and MV8) and surrounding host-rock omphacite have similar trace-element characteristics (Figs 9a and 10, Electronic Appendix 4). In both samples, vein and host-rock omphacite grains have 20–70 ppm Sr, 0·3–0·8 ppm Zr, 0·1–0·5 ppm Pb and low contents of Nb (<0·015 ppm), As (<0·07 ppm) and Sb (<0·07 ppm). Chromium contents are almost exclusively less than 15 ppm, and B contents range from 0·3 to 1·4 ppm (Fig. 10a). Host-rock omphacite from sample MV3 is richer in REE + Y, and poor in V and Co compared with host-rock omphacite from sample MV8 (Fig. 10b and c). None the less, in both of these samples, vein omphacite has similar REE + Y contents to the respective host-rock omphacite. Clear elemental differences between omphacite types are seen only for Li and Co, with vein omphacite poorer in Co and Li than the respective host-rock omphacite (Fig. 10c). It is important to note that the relative differences in Co and Li contents between vein and host omphacite are similar in both samples, despite their considerable differences in absolute element concentrations.

Type-2 veins

Clinopyroxene, garnet and rutile from Type-2 veins have much greater chemical complexity than counterparts from host-rocks or Type-1 veins. To assess the trace element chemistry of Type-2 vein minerals in detail, we acquired nearly 200 clinopyroxene (approximately half of which are Cr-rich domains), >60 garnet, and >60 rutile trace element analyses. For comparative purposes, we also analysed the trace element compositions of minerals in host eclogite adjacent to Type-2 vein samples. Data are presented in Electronic Appendix 4.

Clinopyroxene

Clinopyroxene analyses were conducted using a 60 μm laser beam to lower the limits of element detection; this beam diameter is larger than the dimensions of zoning in most crystals. Thus, most of the LA-ICP-MS analyses include multiple zones and, hence, precise comparison of the trace element chemistry with any single major component (e.g. jadeite, diopside, aegirine) of omphacite is not feasible. Calculation of meaningful trace-element partition coefficients between omphacite and other phases is also

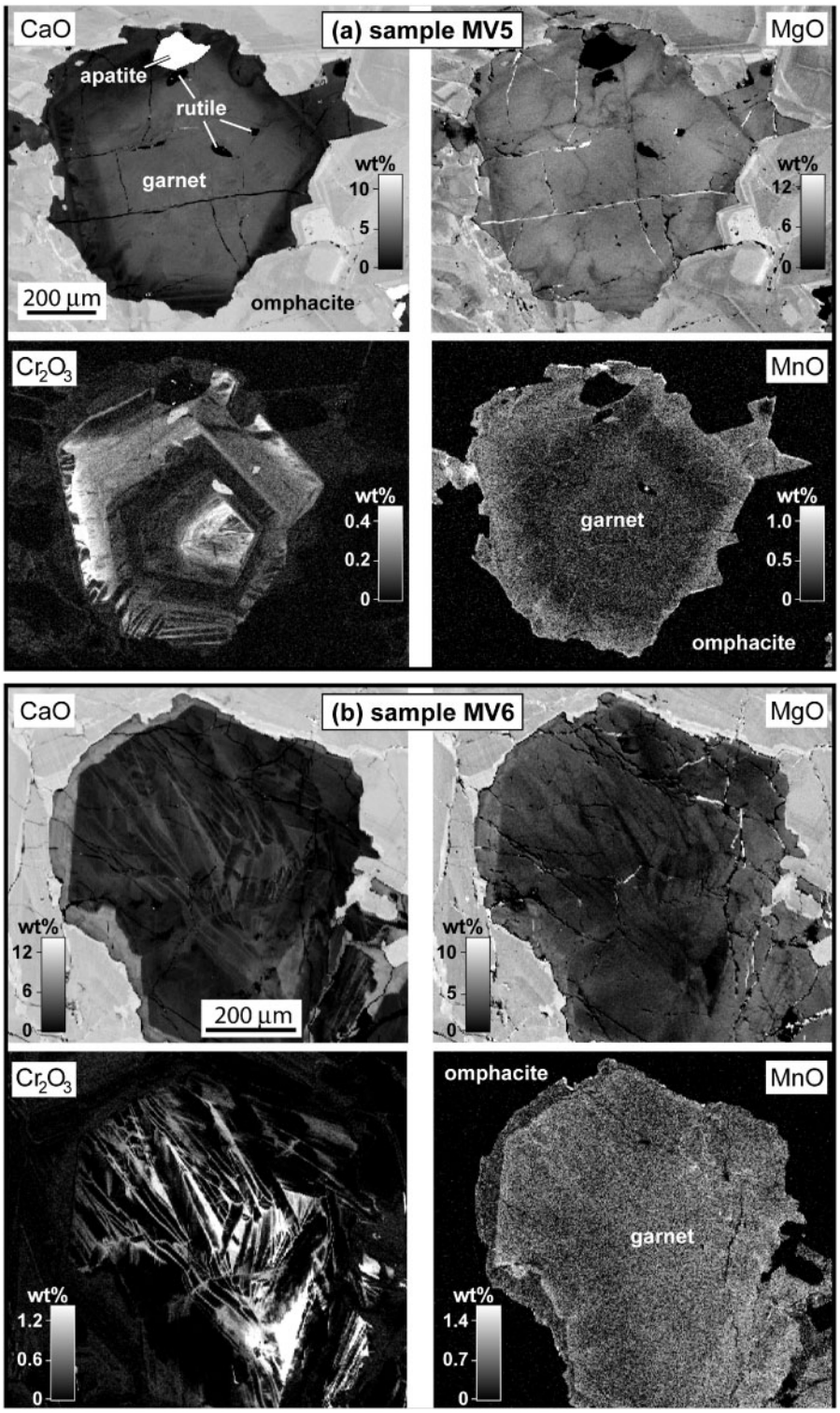

Fig. 6. X-ray intensity maps of Ca, Mg, Cr and Mn in garnet from Type-2 vein samples MV5 (a) and MV6 (b). In garnet from sample MV5 smooth core to rim zoning in Ca and Mn can be observed, whereas the Cr map features oscillatory zoning, with multiple and complex Cr-rich zones. Garnet in sample MV6 shows a chaotic zoning pattern in Cr, Ca and Mg, with a later overgrowth of low-Cr, low-Mn, high-Ca, high-Mg garnet (see also Electronic Appendix 1 for additional X-ray maps of garnet grains). It should be noted that oscillatory zoning in Ca and Mg can also be observed in the omphacite surrounding the garnet in both samples.

not feasible. Nevertheless, we can use chemical proxies to examine the general trace-element behaviour with changing major element composition of omphacite. We use the CaO + MgO content as a proxy for the diopside component. The Cr and Al contents are considered to be direct measures of the kosmochlor and aluminous pyroxene components, respectively.

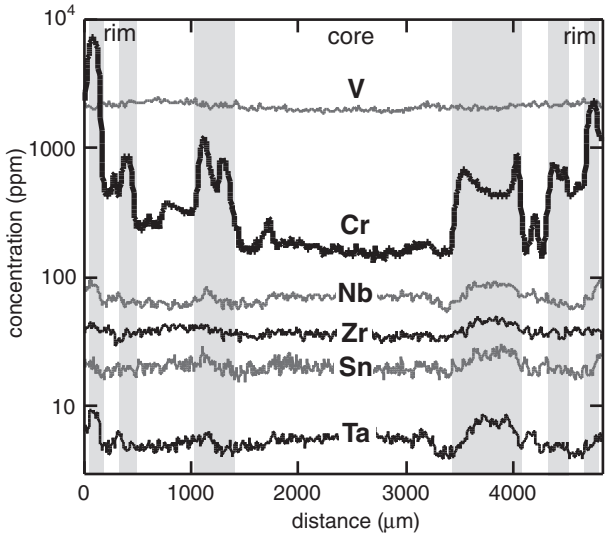

Fig. 7. Trace element profile across (perpendicular to *c*-axis) a large (~0·5 mm wide by ~2 mm long) rutile crystal from Type-2 vein sample MVrut. The data were collected by scanning laser ablation ICP-MS. The large variation in Cr concentration with respect to other elements should be noted. Grey shaded bands indicate zones of relatively high Cr concentration.

In general, Type-2 vein omphacite has larger variations in trace element concentrations than the host-rock omphacite, although there is some overlap in the ranges of trace element contents between each omphacite type (Fig. 11). Lithium in host-rock omphacite extends to higher concentrations than does Li from Type-2 vein omphacite, a feature also observed in Type-1 veins (Fig. 10c). Lithium and Al_2O_3 contents correlate in Type-2 vein omphacite (Fig. 11a), signifying that Li substitutes into pyroxene as a spodumene ($LiAlSi_2O_6$) component. Broad positive correlations with CaO + MgO indicate that Sr (Fig. 11b), light to middle REE (LREE–MREE) (Fig. 11c), Co and, to some extent, Ni partition with the diopside component of the pyroxenes.

Chromium contents of host-rock omphacite may reach 1000 ppm; however, Cr is below 20 ppm in most samples (see Electronic Appendix 4, which is available for downloading at http://www.petrology.oxfordjournals.org). Most Type-2 vein omphacite grains have relatively low kosmochlor components, with Cr contents between 50 and 1000 ppm (Fig. 11). These crystals have similar trace element compositions to the host-rock omphacite (Figs 9 and 11d–i). Chromium contents of kosmochlor-rich omphacite measured by LA-ICP-MS reach wt % levels, which agrees well with electron microprobe analyses. The concentration of many trace elements (Pb, Sr, REE, Ti, Co) is similar in both Cr-rich and Cr-poor vein omphacite (Fig. 9). Scandium and V contents vary over several orders of magnitude in Cr-rich vein omphacite (e.g. Fig. 11d), but there is no clear relationship between V and Sc or any other trace element. Boron, As and Sb contents of both host-rock

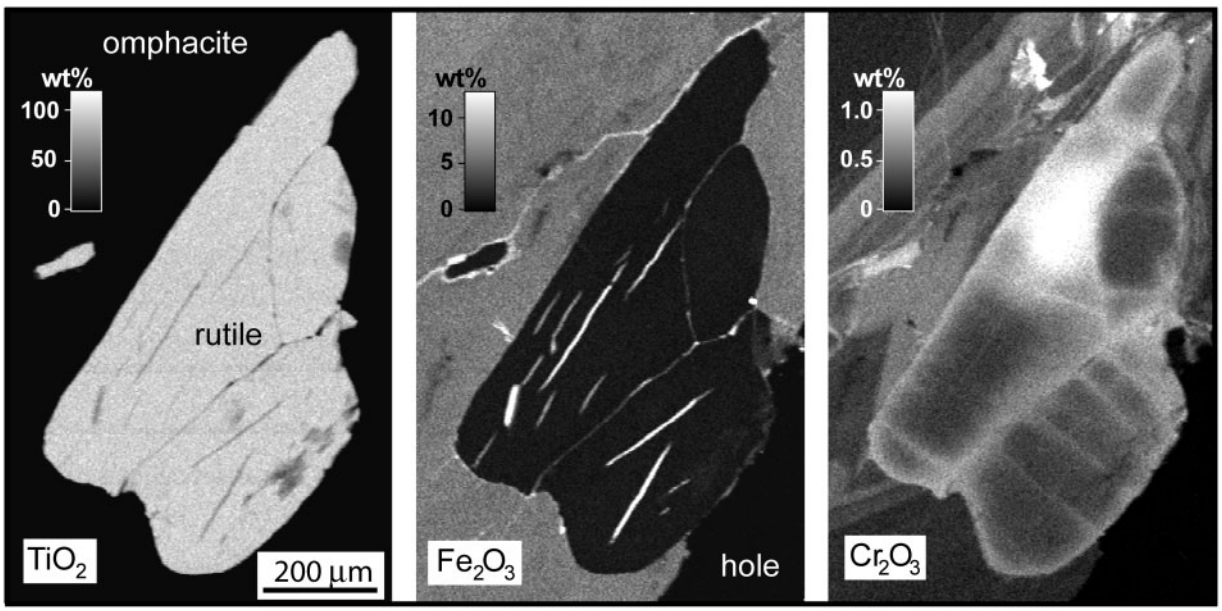

Fig. 8. X-ray intensity maps of TiO_2, Fe_2O_3 and Cr_2O_3 in rutile from Type-2 vein sample MV6. The high-Fe zones are ilmenite exsolution lamellae. The Cr zonations pattern should be noted; this resembles Cr zonation features found in garnet crystals in this sample (Fig. 6b).

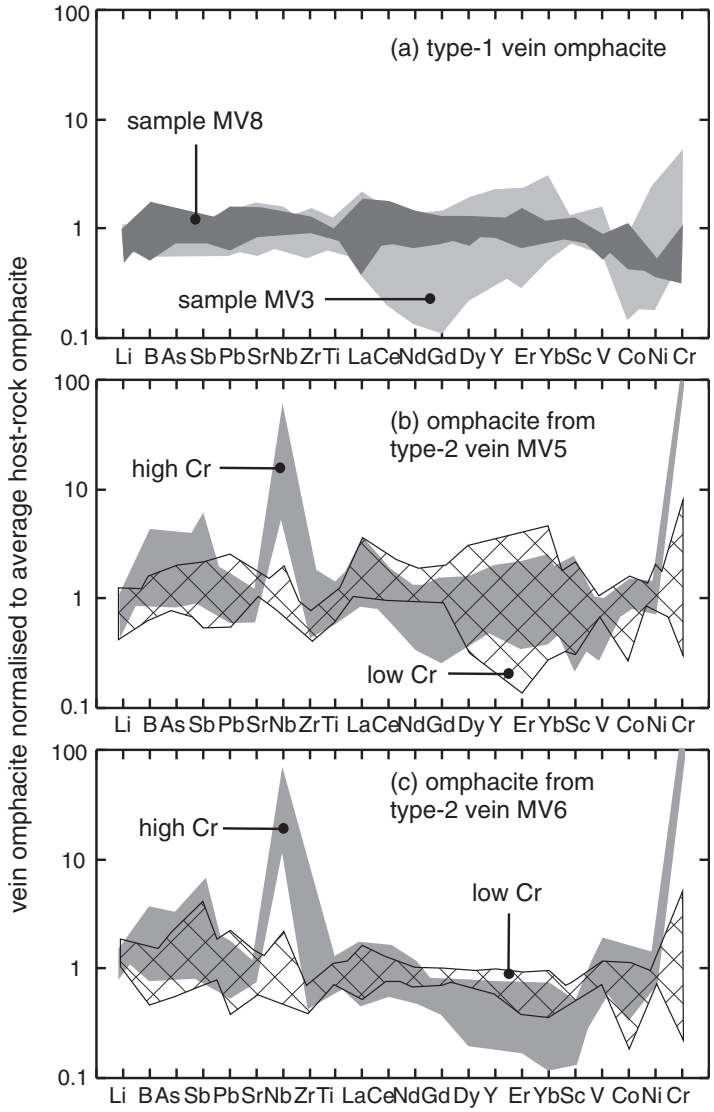

Fig. 9. Trace element variation diagrams for omphacite from selected vein samples. The data are normalized to the average composition of omphacite from the host-rock adjacent to each of the veins. (a) Omphacite from Type-1 vein sample MV3 (light grey field) and MV8 (dark grey field); (b) and (c) omphacite from Type-2 vein samples MV5 and MV6, respectively. The fields for low-Cr (<1000 ppm) and high-Cr (>10,000 ppm) Type-2 vein omphacite are plotted separately as hatched and filled grey fields, respectively.

and low-Cr vein omphacites are relatively low, with many analyses below the respective element detection limits. Host-rock omphacite shows a broad trend of decreasing B, As and Sb with increasing Cr (Fig. 11e–g). In contrast, kosmochlor-rich omphacite domains show B, As and Sb contents that range from values typical of, to values many times higher than, host-rock omphacite (Fig. 9). It is important to note that kosmochlor-rich (>1 wt % Cr) omphacite with high B, As and Sb is found in Type-2 vein samples from both localities examined.

Zirconium has similar characteristics to As, B and Sb, with Zr concentrations of over 2 ppm in some kosmochlor-rich vein omphacite. The element best correlated with Cr is Nb (Fig. 11h). Host-rock and low-Cr vein omphacites have Nb contents less than 0·02 ppm, whereas all Cr-rich omphacite domains are also Nb rich (Fig. 9), with concentrations up to 0·25 ppm. Niobium does not correlate with TiO_2; hence, elevated Nb contents in omphacite do not result from accidental ablation of rutile inclusions during analysis. Rare earth element and Y contents do not correlate with Cr, but Cr-rich omphacite commonly features elevated LREE/MREE (Fig. 11i).

Garnet

Garnet grains from both the host-rock and Type-2 veins have low contents of most incompatible trace elements

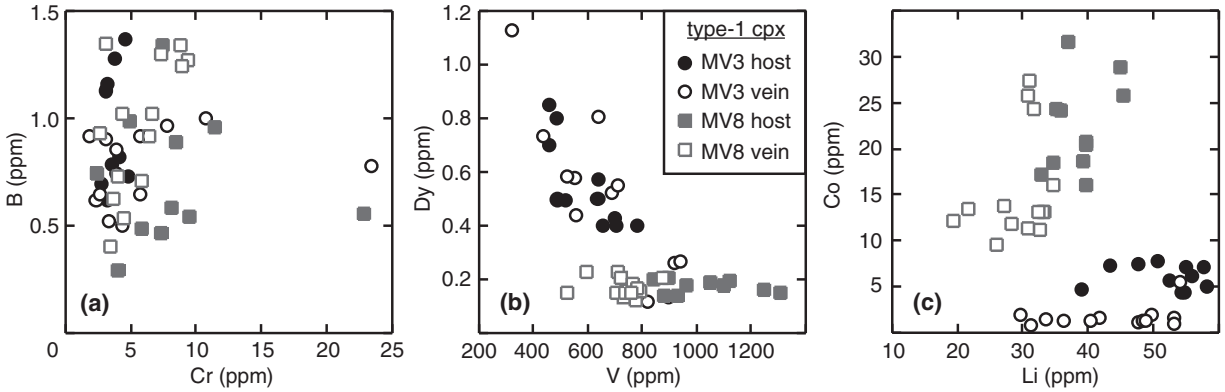

Fig. 10. Selected trace element characteristics of omphacite from the Type-1 veins and adjacent host eclogites. (a) B vs Cr; (b) Dy, vs V; (c) Co vs Li. Type-1 vein omphacite trace element data are reported in Electronic Appendix 4.

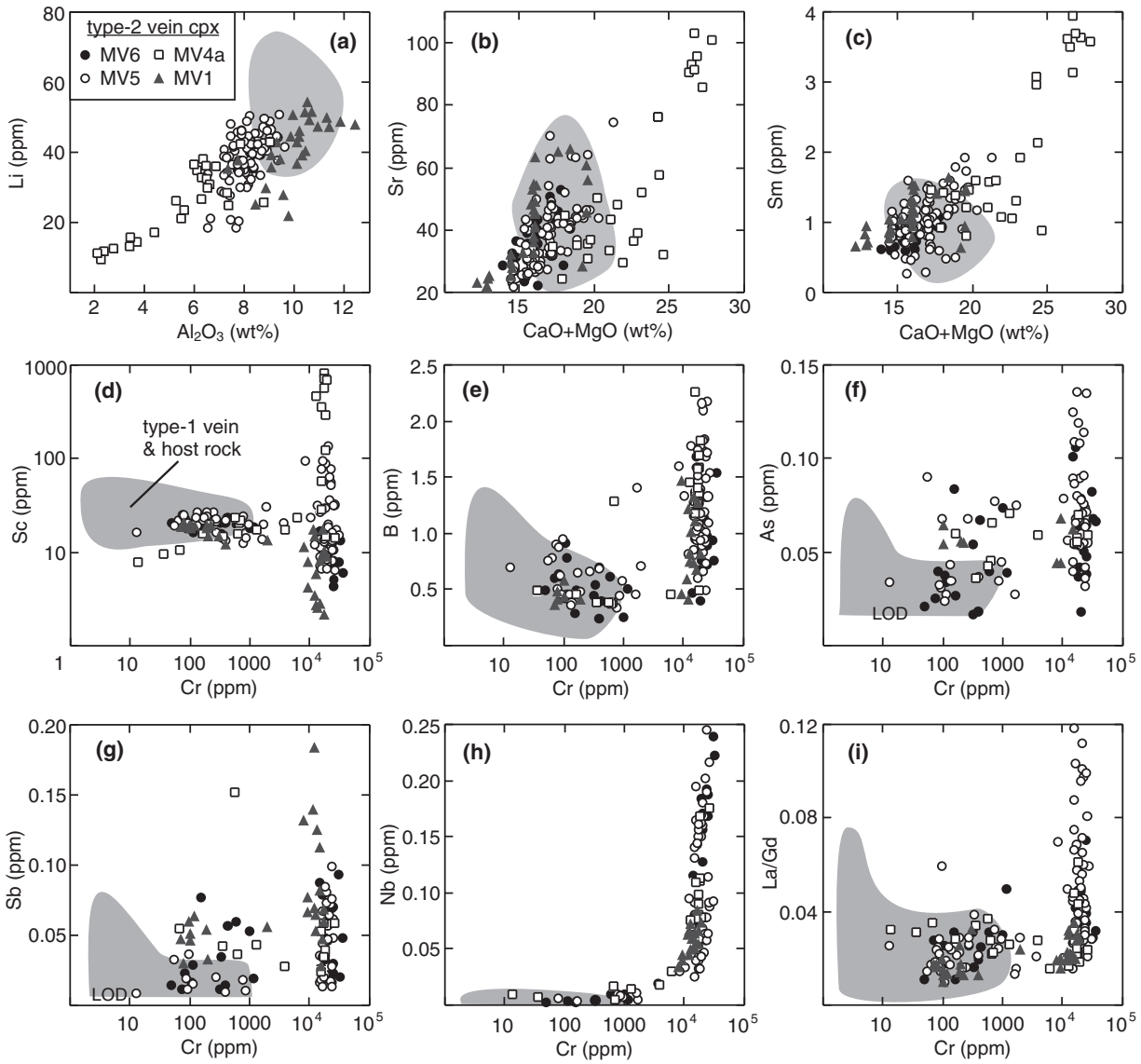

Fig. 11. Selected trace element characteristics of Type-2 vein omphacite compared with host-rock and Type-1 vein omphacite (grey fields). (a) Li vs Al_2O_3; (b) Sr vs CaO + MgO; (c) Sm vs CaO + MgO; (d) Sc vs Cr; (e) B vs Cr; (f) As vs Cr; (g) Sb vs Cr; (h) Nb vs Cr; (i) La/Gd vs Cr. LOD, limit of detection. It should be noted that both log and linear scales are used in this figure. Omphacite trace element data are reported in Electronic Appendix 4.

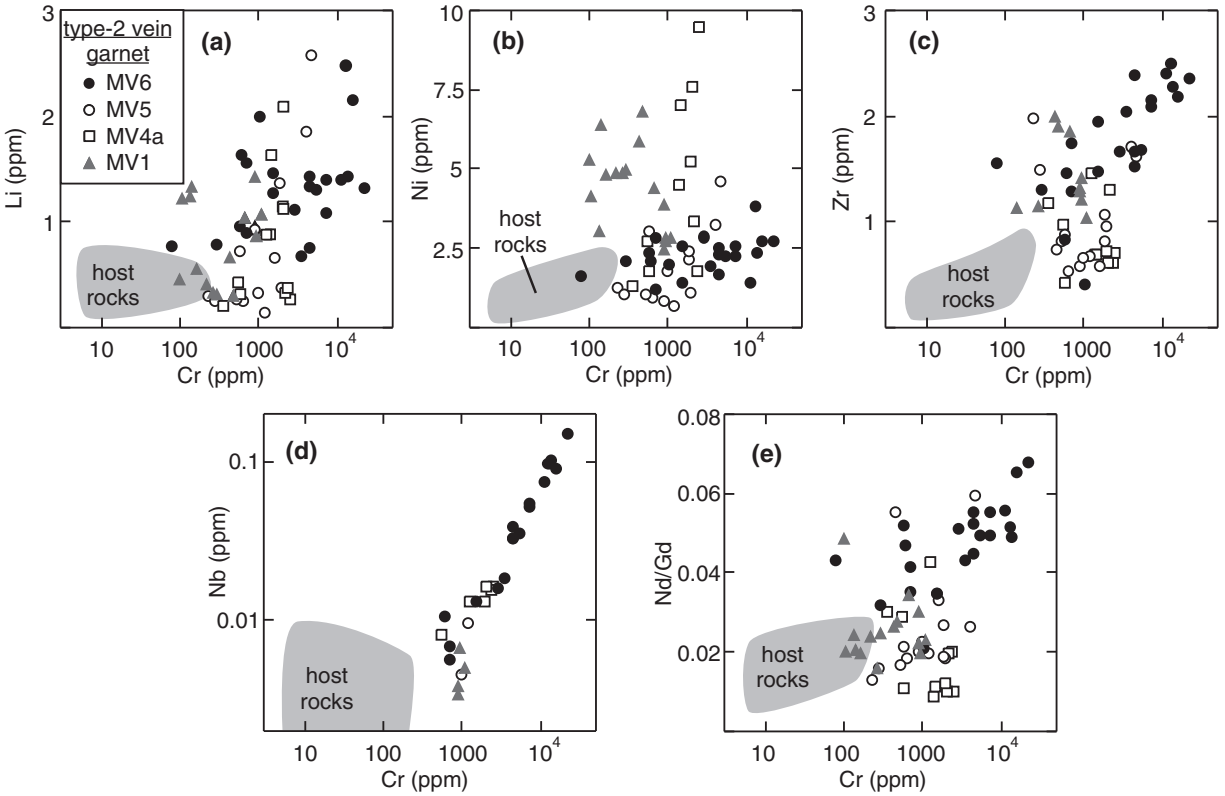

Fig. 12. Selected trace element characteristics of garnet from Type-2 veins and host eclogites. (a) Li vs Cr; (b) Ni vs Cr; (c) Zr vs Cr; (d) Nb vs Cr; (e) Nd/Gd vs Cr. It should be noted that both log and linear scales are used in this figure. Grey fields represent host-rock garnet compositions. Garnet trace element data are reported in Electronic Appendix 4.

(Electronic Appendix 4). Lead, Sr and LREE contents are below 0·2 ppm, and B, As, and Sb contents are below their respective detection limits of around 0·5, 0·1 and 0·05 ppm. Garnet MgO content directly correlates with Co concentration and CaO correlates with V. Yttrium and REE correlate with MgO in host-rock garnet, whereas there is no clear relationship between these trace elements and any major element components of vein garnet.

Host-rock garnet contains up to 200 ppm of Cr, but Cr contents are typically less than 20 ppm. In contrast, vein garnet has considerably higher Cr contents of up to 25 000 ppm (Fig. 12). Vein garnet also tends to be rich in Li, Ni and Zr compared with host-rock garnet (Fig. 12a–c), and Zr clearly correlates with Cr content. Niobium contents were mostly below detection limits, although some Cr-rich vein garnets (samples MV6 and MV4a) have relatively high Nb contents that correlate well with Cr (Fig. 12d). All types of vein garnet show variable degrees of enrichment of LREE over MREE (Fig. 12e) relative to the host-rock garnet, a feature that is most apparent in Cr-rich garnet from sample MV6. The Y and HREE contents of vein garnet are variable and do not correlate with Cr.

Rutile

As with garnet and omphacite, rutile from Type-2 veins is richer in Cr than rutile from the surrounding eclogite host-rocks (Fig. 13; Electronic Appendix 4). Elements that partition strongly into rutile, such as Nb and V, span a large compositional range in both vein and host-rock rutile (Fig. 13a). A centimetre-sized rutile crystal from a Type-2 vein (sample MVrut) is depleted in Nb and enriched in V compared with other Type-2 vein rutiles. Chromium-rich zones within single crystals are also rich in Nb, Ta and, to a lesser extent, Zr and Sn (Fig. 7). Both vein and host-rock rutile grains have 30–40 ppm Zr and <1 ppm Co. Nickel and Sb contents are generally less than 30 ppm and 2 ppm, respectively, although some Cr-rich vein rutile grains contain up to 80 ppm Ni (Fig. 12b) and 4 ppm Sb (Fig. 12c).

Zircon and talc

The REE, Y, Th and U geochemistry of zircon crystals from Type-2 veins has previously been investigated by Rubatto & Hermann (2003). We analysed the same zircon grains for a range of additional trace elements. Chromium is highly incompatible in zircon, with previous

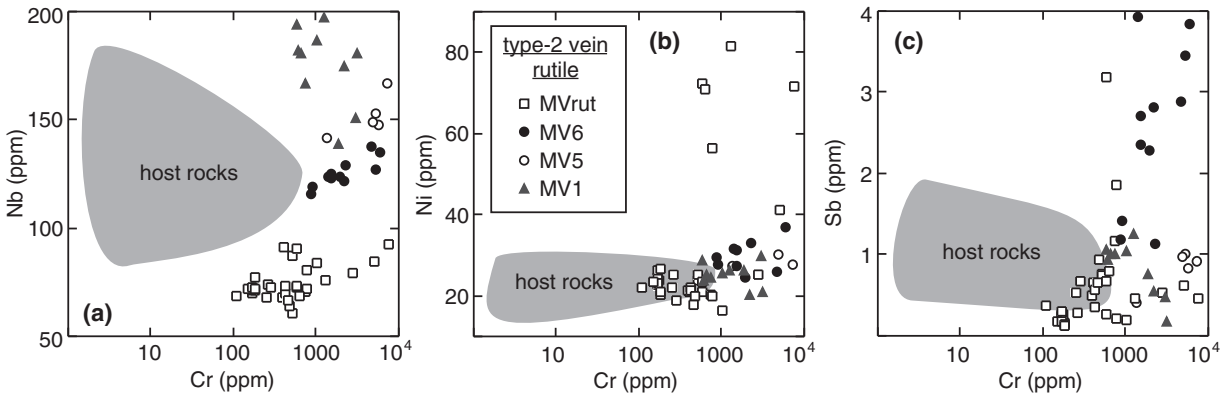

Fig. 13. Selected trace element characteristics of rutile from Type-2 veins and host eclogites (grey fields). (a) Nb vs Cr; (b) Ni vs Cr; (c) Sb vs Cr. Rutile trace element data are reported in Electronic Appendix 4.

studies only finding concentrations below 0·5 ppm (Hoskin & Schaltegger, 2003). None the less, we have measured 1–2 ppm Cr in the Type-2 vein zircon (Electronic Appendix 4). Niobium contents of zircon are between 8 and 9 ppm and Ni, B, As, and Sb are below detection limits. Talc that appears to coexist with omphacite in vein sample MV5 has low contents of almost all trace elements, with the exception of ~5 ppm Li, 5–10 ppm Cr, ~80 ppm Co and between 2000 and 3000 ppm Ni.

ZIRCON Hf ISOTOPE RESULTS

In situ Hf isotope compositions of zircon from both host-rocks and Type-2 veins are presented in Table 6. $^{176}Lu/^{177}Hf$ ratios of vein zircons are $(3–6) \times 10^{-5}$, which are around two orders of magnitude lower than those for the zircons of igneous origin from the host-rock. This reflects the strong depletion in Lu with respect to Hf in vein zircon, which has been attributed to co-crystallization of garnet (Rubatto & Hermann, 2003; Zheng *et al.*, 2005), a phase that heavily sequesters HREE. Measured $^{176}Hf/^{177}Hf$ ratios of zircons from the Type-2 vein and its host-rock are similar within error. Calculated to the age of vein formation (45 Ma; Rubatto & Hermann, 2003), vein zircons tend to have more radiogenic ε_{Hf} values (12·4–13·6) compared with the host-rock zircons (9·2–12·4), although the two groups just overlap within error (Table 6).

DISCUSSION

Evolution of the eclogitic host-rocks

Nd–Hf isotopic data from Duchêne *et al.* (1997) indicate that the Lago Superiore eclogitic rocks originally formed in a mid-ocean ridge environment. The bulk-rock geochemistry of the mylonitic eclogites is consistent with an origin as evolved ocean-floor gabbros (Table 2), and the rocks preserve magmatic zircons (Rubatto & Hermann, 2003) with MORB-like Hf isotope compositions (Table 6; Chauvel & Blichert-Toft, 2001). The eclogites have relatively high TiO_2 and Fe_2O_3 contents and probably originally comprised a magmatic assemblage of plagioclase, pyroxene and ilmenite/Ti-rich magnetite, as is reported in ferrogabbros and ferrobasalts of modern oceanic crust (e.g. Perfit & Fornari, 1983; Natland *et al.*, 1991; Ozawa *et al.*, 1991). Subsequent alpine metamorphism to an eclogite-facies assemblage yielded large proportions of rutile and garnet.

Relatively low $\delta^{18}O$ compositions and highly saline fluid inclusions have been cited as evidence that these gabbros underwent high-temperature hydrothermal alteration prior to subduction (Barnicoat & Cartwright, 1997; Philippot *et al.*, 1998). The geochemistry of the eclogite samples varies significantly (Table 2), even down to the centimetre scale, which may reflect primary heterogeneities owing to cumulate layering and/or ocean-floor hydrothermal alteration. Despite these variations, it is important to note that the concentrations of Cr and Ni in the rocks (Fig. 3) and their constituent minerals (Figs 10–13) are always fairly low. Cr and Ni are regarded as among the most immobile of elements during ocean-floor alteration (Hart *et al.*, 1974; Bach *et al.*, 1996) so these low concentrations are likely to be primary features of the igneous protolith.

Hf isotope compositions of vein and host-rock zircon crystals

The vein and host-rock igneous zircon have similar Hf isotope compositions, with the vein having marginally higher ε_{Hf} at 45 Ma (Table 6) with respect to the host-rock zircons. Zircon and garnet respectively host >90% and <2% of the Hf budget of the Monviso eclogites and veins (Rubatto & Hermann, 2003) and the igneous zircon in the host-rocks exhibits textures indicative of partial alteration by fluids (see Rubatto & Hermann, 2003, fig. 4a). Therefore, we conclude that the bulk of the vein zircon grew from locally derived fluids that had dissolved

Table 6: Zircon Lu–Hf isotopic data for Lago Superiore eclogite and Type-2 vein

	$^{176}Lu/^{177}Hf$	2SE	$^{176}Hf/^{177}Hf$	2SE	$^{176}Hf/^{177}Hf_{(i)}$	$\varepsilon_{Hf(i)}$	2SE
Host eclogite							
E-1	0·0040	0·00001	0·28303	0·00003	0·28304	10·5	1·1
E-2	0·0045	0·00006	0·28309	0·00004	0·28310	12·4	1·4
E-3	0·0031	0·00002	0·28302	0·00005	0·28303	10·2	1·7
E-4	0·0037	0·00001	0·28299	0·00005	0·28300	9·2	1·8
E-5	0·0058	0·00019	0·28304	0·00006	0·28305	10·9	2·2
Average	0·0042	–	0·28304	–	0·28305	10·6	1·6
Type-2 vein							
V4-1	0·00005	0·000001	0·28310	0·00002	0·28311	13·0	0·7
V4-2	0·00004	0·000001	0·28309	0·00002	0·28310	12·6	0·8
V4-3	0·00003	0·000001	0·28310	0·00002	0·28311	12·9	0·8
V4-4	0·00006	0·000001	0·28312	0·00005	0·28313	13·6	1·6
V4-5	0·00003	0·000001	0·28308	0·00002	0·28309	12·4	0·8
V4-6	0·00003	0·000001	0·28311	0·00002	0·28312	13·4	0·8
Average	0·00004	–	0·28310	–	0·28311	13·0	0·9
Depleted mantle*	0·03899	–	0·28321	–	0·28320	15·2	–

i = 45 Ma, which corresponds to the age of vein zircon formation (from Rubatto & Hermann, 2003). 2SE = 2 × standard deviation.
*Values for depleted mantle come from average $^{176}Hf/^{177}Hf$ of Pacific and Atlantic MORB and model mantle source calculations of Chauvel & Blichert-Toft (2001). Sample details have been outlined by Rubatto & Hermann (2003).

host-rock zircon. The tendency to higher ε_{Hf} values in the vein zircon with respect to the country rock zircons, however, requires an additional source of more radiogenic Hf. Garnet preferentially incorporates Lu over Hf, so garnet can develop a highly radiogenic Hf isotope composition over a relatively short time period (e.g. Smith & Griffin, 2005; Zheng *et al.*, 2005). The presence of atoll garnets in the eclogite host-rocks is evidence for garnet dissolution by fluids (e.g. Cheng *et al.*, 2007), so the component of radiogenic Hf in the vein zircons may derive from host-rock garnet. An alternative source of the radiogenic component is external fluids from the nearby serpentinites, which probably followed a depleted mantle Hf evolution, and so had significantly higher $^{176}Hf/^{177}Hf$ than the eclogitic host-rocks at the time of vein formation (see Table 6). In summary, the slight enrichment in radiogenic Hf in the vein zircons is in line with formation from locally derived fluids, but does not exclude the hypothesis that external fluids deriving from a primitive source contributed to vein formation.

Formation of the veins

Both Type-1 and Type-2 veins consist of eclogite-facies minerals, but lack the mylonitic fabric seen in the eclogite host-rocks. Temperatures of metamorphism were below those required for fluid-saturated melting of mafic rocks (Lambert & Wyllie, 1972), so the veins were produced by subsolidus fluid–rock interaction under eclogite-facies conditions. Previous studies (Philippot & Kienast, 1989; Philippot & Selverstone, 1991; Philippot & van Roermund, 1992; Nadeau *et al.*, 1993) all suggested that the veins predominantly formed from locally derived fluids, with fluid movement restricted to the centimetre scale or less (Philippot & Selverstone, 1991; Nadeau *et al.*, 1993). Veins grew by a combination of repetitive crack-sealing of mineral grains and diffusional mass transfer in an immobile fluid that was wetting mineral surfaces (Philippot & Selverstone, 1991; Philippot & van Roermund, 1992). These studies found little evidence for the involvement of external fluids in vein formation. A notable exception is the finding of Philippot & Kienast (1989) of kosmochlor-rich clinopyroxene as inclusions in vein garnet or as cores of vein omphacite, which suggests that external fluid infiltration may have occurred at a relatively early stage of vein formation.

This study further constrains the conditions under which the veins formed. Type-1 veins are little deformed and consist largely of coarse fibrous omphacite. We concur with Philipott & Kienast (1989) that these veins developed as syntaxial crack-seal fractures during mylonitic deformation of the host-rocks. The Type-1 omphacite is similar in composition to omphacite from the immediate host-rock

(Fig. 10). However, trace-element characteristics vary between different vein–host-rock pairs. These observations indicate that omphacite in Type-1 veins and their host-rocks are chemically equilibrated, at least on the centimetre scale, which supports prior conclusions that Type-1 veins formed from fluids sourced from the adjacent eclogite. Dissolution–precipitation processes induced little change in the trace element composition of the omphacites, with the exception of their Li and Co contents, which are slightly depleted in the veins compared with their host-rocks (Fig. 10c).

The deformed and discontinuous nature of the Type-2 veins and their crosscutting relationship with the host-rock fabric prevents assessment of the original vein dimensions, but does indicate that this vein type had a protracted and complex evolution. The deformation history of the veins is also evident in thin section by the randomly oriented blocky and fine-grained foliated omphacite types, which are interpreted to form in veins during shearing-induced dynamic recrystallization of vein minerals (see Philippot & van Roermund, 1992; Oliver & Bons, 2001). The late-stage fractures filled with coarse bladed omphacite in the Type-2 veins (see Electronic Appendix 1) texturally resemble the Type-1 veins, although timing relations place this fracture filling generation to be later than most Type-1 veins (Philippot & Kienast, 1989). These observations indicate that both vein types have complex but contemporaneous growth histories, and are in agreement with the model of Philippot & van Roermund (1992) that invokes vein formation during an HP-deformation history that involved repeated cycling between plastic deformation and fracturing.

Most (>90%) Type-2 vein omphacite grains have similar compositions to omphacite from the host eclogite (Fig. 11), so we suggest that these veins predominantly formed from locally derived fluids. Our Hf isotope data are also consistent with a local fluid source for zircon in these veins. However, Type-2 veins do contain Cr-rich zones in clinopyroxene, garnet and rutile, equivalents of which are not present in the enclosing host eclogite. Kosmochlor-rich clinopyroxene described from other geological settings is associated with ultramafic rocks and is usually interpreted to form as a replacement of Cr-rich spinel (e.g. Harlow & Olds, 1987; Ikehata & Arai, 2004; Tsujimori & Liou, 2004). Likewise, Cr-rich zones within garnet from semi-pelitic schists reported by Martin (2009) were attributed to highly localized sourcing of components for garnet growth from neighbouring mineral phases in the rock matrix. Magnetite was probably part of the original igneous paragenesis of the Fe–Ti eclogites, but it would have been Cr-poor (Natland *et al.*, 1991; Ozawa *et al.*, 1991). This is consistent with the low Cr contents of all constituent minerals in the Fe–Ti eclogites, so there is no reason to suppose the presence of any precursor Cr-rich minerals in these rocks. A purely replacement origin for the Cr-rich domains is difficult to reconcile with their occurrence in multiple mineral phases and is also inconsistent with the chemical zoning and trace element characteristics of the vein minerals (see below). In contrast, all of the available evidence indicates that the Cr-rich mineral zones were formed from solutes advected in a fluid phase.

Kosmochlor-rich clinopyroxene can occur in any section of omphacite, including grain cores, grain rims and cutting pre-existing omphacite zoning or grain boundaries (Fig. 2, Electronic Appendix 1). These textures support multiple episodes of Cr-rich clinopyroxene growth via recrystallization of pre-existing omphacite by Cr-bearing fluids. However, the Cr-rich zones occur exclusively in omphacite domains that have undergone shearing and recrystallization, which has resulted in a near-random distribution of Cr-rich zones at the sub-millimetre scale. The assemblage of Cr-rich minerals, together with the observation that the Cr-rich zones of garnet and rutile are enclosed by later generations of these minerals (Figs 6 and 7), suggests that growth of the Cr-rich zones occurred under eclogite-facies conditions.

In Type-2 vein sample MV4a there is a broad negative correlation between the molar aegirine and kosmochlor components (Fig. 4b), which is consistent with exchange of Fe^{3+} by Cr^{3+} in the pyroxene in response to Cr-rich fluid alteration. Vein garnet is richer in pyrope and Cr than the host-rock garnet, and vein rutile is commonly richer in Cr than the host-rock rutile. The two distinct types of chemical zoning preserved in garnet and rutile may reflect different mechanisms of precipitation from fluid. We expect that these zoning features are well preserved in garnet and rutile, but not omphacite, owing to the resistance of garnet and rutile to recrystallization during shear deformation. The fracture-like texture of garnet (and probably rutile) as observed in samples MV4a and MV6 (Fig. 6; Electronic Appendix 1) probably formed by multiple episodes of crack-sealing of these grains during fluid influx. Oscillatory zoning of rutile and garnet in samples MV1, MV5 and MVrut is suggested to have formed by precipitation of solutes diffusing through fluid that was wetting grain boundaries. This scenario requires relatively low fluid flux, which may arise in response to resealing of fractures following fluid influx. Similar mechanisms have already been suggested to be primarily responsible for mineral growth in these veins (Philippot & van Roermund, 1992). We interpret the crack-sealing and oscillatory growth zoning of minerals as products of precipitation during conditions of relatively high and low vein fluid pressure, respectively (Oliver & Bons, 2001). Alternation between high and low fluid-pressure regimes was probably linked to transitions between brittle fracturing and shear deformation, respectively (Philippot & van

Roermund, 1992), which also is consistent with textural features observed in the vein samples. Importantly, the mineral zoning structures also indicate that vein formation involved multiple pulses of both Cr-rich and Cr-poor fluids.

Controls on the trace element content of vein minerals

The trace element geochemistry of vein minerals will be influenced by two independent parameters: (1) mineral major element composition; (2) the composition of the fluid phase. Chromium contents of vein clinopyroxene, garnet and rutile reach weight per cent levels and, hence, are likely to induce structural changes to the crystal lattices, which will influence trace element partitioning. Two groups of trace elements can be distinguished in our dataset, those that do not linearly correlate with Cr contents and those that do. Kosmochlor-rich vein clinopyroxene shows variably elevated contents of B, As and Sb and enrichment of LREE over MREE (Figs 9 and 11). Likewise, Cr-rich garnet may have relatively high Ni, Li and LREE/MREE (Fig. 12) and Cr-rich rutile may have elevated Sb and Ni contents (Fig. 13). It is important to note that in all of these cases trace element concentrations vary significantly and there is no clear correlation with Cr content. This result indicates that crystal-chemical effects induced by high Cr contents do not solely control the concentrations of these trace elements. Moreover, some components are enriched in more than one Cr-rich mineral phase, such as Sb in both clinopyroxene and rutile, LREE/MREE in clinopyroxene and garnet, and Ni in garnet and rutile (and talc), thus excluding simple changes in element partitioning as the cause for elevated contents.

Niobium and Zr contents correlate directly with Cr concentration in both clinopyroxene (Fig. 11h) and garnet (Fig. 12c and d), which indicates that these elements may have some crystal-chemical relationship with Cr. Under equilibrium conditions, the Zr contents of these minerals should be buffered by the vein zircon, which would further support crystal-chemical control on Zr. Nb and Ti budgets in eclogitic rocks are almost exclusively controlled by rutile (Zack *et al.*, 2002; Rubatto & Hermann, 2003), so the large variation in the Nb contents between samples (Fig. 13a) reflects variations in the TiO_2/Nb of the bulk-rocks. Nevertheless, in most vein rutile Nb and Cr contents increase together (Figs. 7 and 13a). Therefore, a direct relationship between Nb and Cr exists in the three major vein minerals. Moreover, Cr-rich clinopyroxene and garnet domains are often associated with rutile inclusions, indicating co-precipitation of these phases.

With crystal-chemical controls considered, we can now use the trace element composition of the Cr-rich mineral phases to qualitatively assess the composition of the fluid responsible for the precipitation of these Cr-rich vein minerals. We conclude that this fluid was not only rich in Cr, but also rich in Ni, B, As, Sb and LREE/MREE. Scandium and V contents vary in all Cr-rich phases, indicating that these elements may be influenced by multiple parameters. Nb may also have been enriched in the fluid phase, although we cannot rule out that crystal-chemical effects dominate its incorporation. The presence of talc, pyrope-rich garnet, zircon and rutile in the veins indicates significant mobilization of Mg and high field strength elements (HFSE), as previously noted by Philippot & Selverstone (1991) and Rubatto & Hermann (2003).

Sources of fluids forming the Cr-rich mineral zones

Multiple generations of Cr-rich and Cr-poor clinopyroxene, garnet and rutile are present in the Type-2 veins. The Cr-poor mineral phases are consistent with an origin from locally derived fluids, as discussed above. The origin of the fluids from which the Cr-rich mineral phases grew is more difficult to evaluate as the veins have experienced a complex deformation history that has modified the original vein geometries and removed most petrographic features that could be used to trace original fluid pathways. Many trace elements have similar concentrations in both vein and host-rock omphacite (Fig. 9). Nevertheless, there are unique geochemical attributes of the Cr-rich mineral zones that allow us to evaluate potential sources for these fluids. Key observations that require explanation are the association of elevated Ni, B, As, Sb, Nb and LREE/MREE in many of the Cr-rich vein mineral zones and the mobilization of HFSE, Ni and Mg to form rutile and talc in these veins. Only two experimental studies present data on the hydrothermal mobility of Cr and Ni in mafic eclogite (Kogiso *et al.*, 1997; Green & Adam, 2003), with both studies finding that these two elements are among the most fluid immobile of all elements. Given that the Type-2 veins have 1–2 orders of magnitude higher concentration of Ni and Cr than their host-rocks (Table 2), extremely large time-integrated fluid fluxes and pervasive fluid flow would be required to source completely the high levels of Cr and Ni present in the veins from the mylonitic Fe–Ti eclogites (Fig. 3). Such high fluid volumes and flow conditions are inconsistent with not only the textures and geochemistry of both the veins and eclogite hosts but also the findings of other studies on these rocks (Philippot & Selverstone, 1991; Philippot & van Roermund, 1992; Nadeau *et al.*, 1993; Rubatto & Hermann, 2003). The trace element signature of the Cr-rich minerals (Figs 11–13) is also inconsistent with a purely local fluid source, so we conclude that an external fluid input is needed to form these phases. The presence of multiple generations of Cr-rich vein minerals indicates multiple episodes of external fluid influx into the veins.

Possible sources of external fluid are the Mg–Al metagabbro and associated talc schist, or serpentinites. Both units structurally underlie the mylonitic eclogite pods.

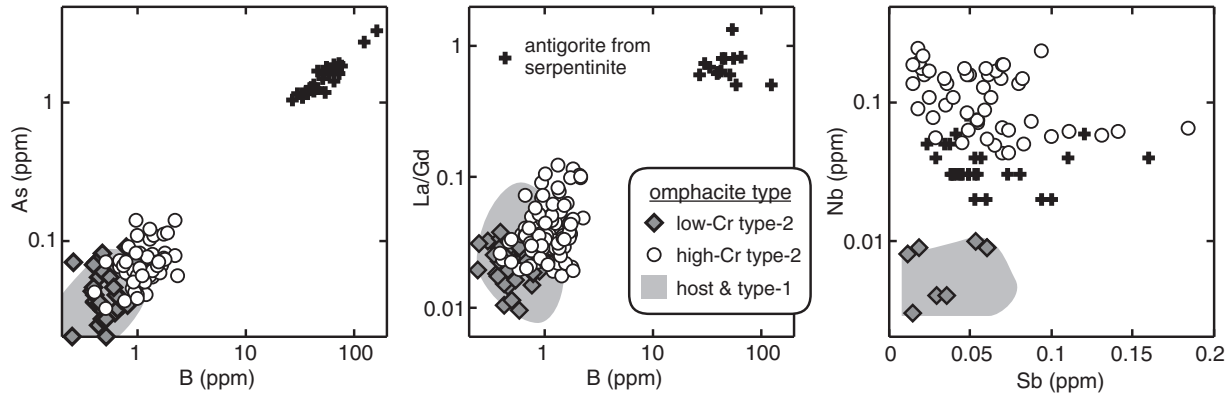

Fig. 14. Variation of As vs B, La/Gd vs B, and Nb vs Sb for omphacite from Monviso host-rock and vein samples and antigorite from Monviso serpentinite. It should be noted that the trend for the high-Cr Type-2 vein omphacite extends away from other omphacite types towards the antigorite compositions. These trends are consistent with the notion that some high-Cr Type-2 vein omphacite precipitated from fluids derived from serpentinite. It is important to note that these trends should not be regarded as simple mixing trends, as the vein materials represent the products of complex hydrothermal alteration processes. All data are available in Electronic Appendix 4.

The Mg–Al metagabbros also contain HP veins (e.g. Nadeau *et al.*, 1993), indicating that fluid-rock interaction operated during metamorphism of these rocks. The Mg–Al metagabbros are rich in Mg, Cr and Ni, but have relatively low B, As and Sb contents (Table 2; see also Hattori & Guillot, 2007). Talc schist bands associated with the Mg–Al metagabbro units are also probably rich in Mg, Cr, Ni and H_2O, although talc dehydration is expected to occur at temperatures far exceeding the peak metamorphic conditions of the Lago Superiore Unit (see Spandler *et al.*, 2008). Talc is also a poor host for elements such as B, Nb, As and Sb (Electronic Appendix 4; Spandler *et al.*, 2008) and so is unlikely to produce the distinctive chemical signature of the Cr-rich vein minerals. Consequently, we propose that fluid addition from Mg–Al metagabbros or talc schists cannot account for all of the trace-element characteristics of the Type-2 vein minerals.

The serpentinite that underlies the eclogitic metagabbros now consists almost completely of antigorite. In the field, the nearest serpentinite outcrops are *c.* 100 m from the Fe–Ti eclogite pods that host the veins. Our data and previous work show that these serpentinites contain high concentrations of not only Mg, Ni and Cr (as is typical of ultramafic compositions), but also B, As, Sb and LREE/MREE (Table 2, Fig. 14, Hattori & Guillot, 2007). This distinctive elemental association is characteristic of serpentinites from a range of geological settings (Scambelluri *et al.*, 2004; Tenthorey & Hermann, 2004; Savov *et al.*, 2005; Agranier *et al.*, 2007; Hattori & Guillot, 2007).

Results of experiments and studies of natural HP-serpentinite bodies demonstrate that dehydration of serpentinite during metamorphism would produce hydrous fluids rich in B, As and Sb (Scambelluri *et al.*, 2004; Tenthorey & Hermann, 2004; Hattori & Guillot, 2007). Other recent experimental work indicates that such fluids may also carry Nb, Zr and LREE (Spandler *et al.*, 2009), which is consistent with the presence of HFSE-rich minerals in veins in other HP-ultramafic bodies (Scambelluri *et al.*, 2001; López Sánchez-Vizcaíno *et al.*, 2009). The degree of Cr and Ni solubility in fluids in ultramafic systems is poorly known, although fluid-induced mobility of Cr from serpentinite into mafic rocks has been documented in other metamorphic terranes (e.g. Nishiyama *et al.*, 1986; Tsujimori & Liou, 2004). Therefore, the distinctive chemical signature of the Cr-rich minerals in the Type-2 veins, as well as the formation of talc, is consistent with formation from fluids derived from serpentinite.

Metamorphic reactions in serpentinite that could have produced the required fluids include the brucite-out reaction or the antigorite-out reaction. Under conditions typical of subduction-zone metamorphism, the antigorite-out reaction in serpentinite would take place at 630–700°C and 2·5–3·0 GPa (Ulmer & Trommsdorff, 1999), which are higher-grade conditions than the maximum P–T proposed for the Lago Superiore Unit (~600°C >2·4 GPa, Schwartz *et al.*, 2000). The preservation of antigorite in nearby serpentinites also argues against complete antigorite dehydration during metamorphism. The serpentinite and mafic rocks of the Lago Superiore Unit are likely to have been coupled during subduction (Blake *et al.*, 1995; Schwartz *et al.*, 2001), so the brucite-out reaction in these serpentinites would have occurred at *c.* 500°C and 1·5–2·0 GPa (Ulmer & Trommsdorff, 1999). The balanced reaction is as follows:

$$\underset{20[Mg(OH)_2]}{\text{brucite}} + \underset{Mg_{48}Si_{34}O_{85}(OH)_{62}}{\text{antigorite}} = \underset{34(Mg_2SiO_4)}{\text{olivine}} + \underset{51(H_2O)}{\text{water}}.$$

The brucite-out reaction occurs under eclogite-facies conditions, and involves breakdown of antigorite (an important host for B, As and Sb; Fig. 14), and thus represents a likely source of aqueous fluid enriched in Cr, B, As and Sb for the Type-2 veins. Such external fluids may have

also contributed to the enrichment in radiogenic ^{176}Hf in the hydrothermal zircons that formed in the vein (Table 6). Petrographic evidence for focused fluid flow from the Monviso serpentinites is limited because of extensive deformation. Nevertheless, rare olivine-bearing veins cutting the serpentinite are interpreted as the products of percolating fluids produced by the brucite-out reaction under eclogite-facies conditions (Groppo & Compagnoni, 2007), as has also been described in other HP–ultramafic terranes (Scambelluri *et al.*, 2001).

Length-scales and mechanisms of fluid flow

Single Cr-rich mineral zones within Type-2 veins rarely exceed several hundred micrometres in size and collectively form only a minor proportion of these veins (Fig. 2). None the less, the mere presence of these zones with their distinct chemical signature has important implications for the conditions and length-scales of fluid flow in eclogitic rocks. Previous workers have argued on the basis of heterogeneities in stable isotope and fluid inclusion compositions that fluid flow within the Lago Superiore veins was limited to the centimetre scale or less (Philippot & Selverstone, 1991; Nadeau *et al.*, 1993; Philippot, 1993), and so the fluid must have been locally derived. Our findings indicate there was also episodic infiltration of external fluids most probably derived from serpentinite, possibly with contributions from Mg–Al metagabbros or talc schists. Although field observations allow only partial constraints to be made on the geometry and extent of each rock unit, outcrop relations require minimum distances of fluid flow of several tens of metres or more if fluid is derived from Mg–Al metagabbros, talc schists or serpentinites. Stark compositional contrasts between vein minerals grown from internal and external fluids are observed on the micrometre scale (e.g. Figs 6–8), which indicates that externally derived fluid was capable of migrating tens of metres into the veins without prior re-equilibration or buffering with the wall rocks. A complete explanation for these features is currently not possible, because little is known about the mechanisms of fluid flow under HP conditions. None the less, our petrographic evidence (Figs 6 and 8) is consistent with previous work (e.g. Philippot & Selverstone, 1991; Philippot & van Roermund, 1992; Widmer & Thompson, 2001), which suggested that repeated micro-cracking and/or solute diffusion through the fluid was responsible for vein growth from internal fluids. Episodic advection of the externally derived fluid may be achieved by hydrofracturing (Davies, 1999; Oliver & Bons, 2001), mobile hydrofractures (Bons, 2001) or porosity waves (Connolly & Podladchikov, 1998). Under these conditions, fluid would be expected to flow at velocities of up to metres per second (Bons, 2001), which would limit buffering or interaction between the fluid and wall rocks. Enhanced fracture propagation may be expected along zones of structural weakness or rheological contrast, such as pre-existing veins (Fig. 15). Clearly, in such a scenario, fluid flow was highly channelized, as is commonly reported in eclogitic rocks (Miller & Cartwright, 2000; Scambelluri & Philippot, 2001; Hermann *et al.*, 2006; Zack & John, 2007; John *et al.*, 2008).

Implications for subduction zone processes

Investigation of remnant subducted slabs such as the Monviso Massif provides opportunities to understand fluid and element recycling through subduction zones, and our results have a number of important implications for subduction zone processes. We present evidence for the infiltration of serpentinite-derived fluids into subducted oceanic crust at depths of 70–80 km. Although serpentinite is now widely recognized as a potential source of water and specific trace elements (B, As, Sb, Li) for arc magmas (e.g. Ulmer & Trommsdorff, 1999; Scambelluri *et al.*, 2004; Tenthorey & Hermann, 2004; Savov *et al.*, 2005; Hattori & Guillot, 2007), there is little direct evidence to support the notion that large-scale serpentinite fluid migration occurs at depth in subducted slabs. Products of HP serpentinite dehydration are rarely preserved at the Earth's surface (e.g. Cerro del Almirez, Spain) and only a few studies have proposed the process of serpentinite-derived fluid infiltration into crustal rocks at HP to UHP conditions (John *et al.*, 2004; van der Straaten *et al.*, 2008; Ferrando *et al.*, 2009). Our results indicate that serpentinite-derived fluids are not only capable of infiltrating at least tens of metres into mafic eclogite with minimal interaction, but also can transport many characteristic subduction signature elements, such as B, As and Sb. At Monviso, the eclogitic veins formed by local fluid–rock interaction were used as pathways for long-distance fluid percolation. This circumstance is probably non-coincidental, and similar situations may arise in subducting oceanic crust where vein arrays created by localized fluid–rock interaction develop into channelways for advecting deep serpentinite-derived fluids over long distances towards the slab–mantle wedge interface (Fig. 15). Rapid and episodic fluid movement along such zones may be a principal cause (or result) of intermediate-depth seismicity (e.g. Davies, 1999; Hacker *et al.*, 2003; John & Schenk, 2006) and, provided that complete equilibration of the fluid during ascent is avoided, may contribute H_2O and trace elements (e.g. B, As, Sb) to arc magmatism.

Other elements transported by fluids to form the Monviso veins include Ti, Zr, Hf, Nb, Cr and Ni. These elements are typically regarded as highly immobile in hydrothermal systems. Other studies have also documented mobility of HFSE under HP and UHP conditions (Sorensen & Grossman, 1993; Scambelluri *et al.*, 2001; Rubatto & Hermann, 2003; Kessel *et al.*, 2005; Spandler & Hermann, 2006; Gao *et al.*, 2007; John *et al.*, 2008; Zhang *et al.*, 2008; López Sánchez-Vizcaíno *et al.*, 2009), indicating

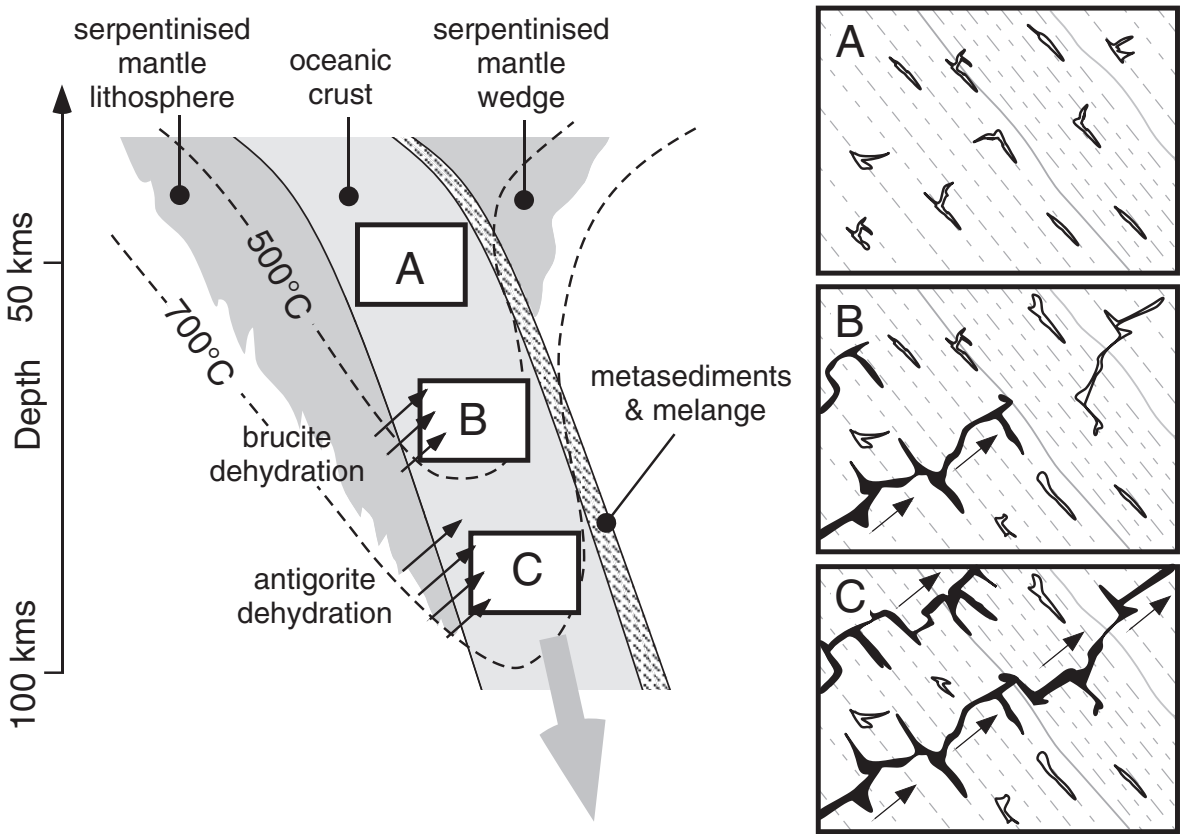

Fig. 15. Schematic illustration of progressive vein development in subducting oceanic crust (not to scale). Region A, closed-system veins (white fill) form in the basaltic eclogite from locally derived hydrous fluids produced by metamorphic devolatilization reactions. These veins continue to develop with progressive subduction and slab dehydration. Type-1 veins at Monviso are representative of this vein type. Interconnection of these veins may allow influx of external fluids, such as fluid produced by brucite breakdown in underlying serpentinized lithospheric mantle, as portrayed by the black-filled veins in region B. We propose this process for the evolution of the Monviso Type-2 veins. At deeper levels (region C), large fluid volumes produced by antigorite dehydration in the lithospheric slab mantle may traverse the eclogitic oceanic crust utilizing these interconnected vein systems (shown with black fill). These fluid channelways may allow rapid transport of hydrous fluids and effective transfer of chemical source signatures into the upper portions of the slab (metasedimentary materials or mélange) or mantle wedge and, hence, may be important for the generation of arc magmas.

that the long-standing assumption of HFSE immobility in HP-slab fluids is not correct. However, the presence, or even abundance, of minerals rich in these elements in veins is, in itself, not evidence for high element solubility in fluids, as the parameters of fluid flux, fluid sources and precipitation mechanisms need also to be considered. HP veins are excellent records of solute precipitation from fluids but provide limited information on solute concentrations in these fluids, and we stress that further work is required to better constrain the element transport capacity of subduction zone fluids.

CONCLUSIONS

Multiple fluid sources are required to explain the genesis of eclogite-facies veins in Fe–Ti metagabbros of the Monviso Massif. Micrometre-scale chemical zonation in vein minerals records episodic influx of externally derived fluids, in addition to dominantly locally derived fluids from which most of the mass of the veins formed. The cryptic nature of these mineral zonations suggests that evidence for multiple fluid sources may be present but well disguised in many vein systems, and we recommend undertaking combined detailed petrographic and chemical characterization of veins, from outcrop to micrometre scales, to aid in evaluating potentially complex vein formation processes.

The chemical signatures (high Cr, Ni, Mg, ± As, ± Sb, ± B) of the externally derived fluids preserved in the Monviso veins indicate serpentinite and, potentially, Mg–Al metagabbro sources, which requires fluid flow of at least tens of metres through the eclogite without extensive fluid–rock interaction. In subducting slabs, such conditions are probably met by short-lived and episodic fracture openings, which may manifest as intermediate- to deep-level seismicity, and may represent an important

mechanism to transfer volatiles and trace elements through the slab.

ACKNOWLEDGEMENTS

We thank Joerg Hermann for discussion of ideas and help in the field, and Nick Oliver for comments on an early version of the paper. Alfons Berger, Tanya Ewing, Lydia Zehnder and Alexey Ulianov are thanked for assistance with X-ray mapping, Hf isotope data, XRF and LA-ICP-MS analysis of di-lithium tetraborate glass tablets, respectively. Thorough reviews by Sorena Sorensen, Kevin Klimm, Axel Liebscher and two anonymous reviewers resulted in significant improvements to the paper.

FUNDING

This study was funded by the Swiss National Science Foundation (grant PP002-106569 to T.P.). D.R. and C.S. acknowledge the support of the Australian Research Council (DP 0556700 and DP 1095280).

SUPPLEMENTARY DATA

Supplementary data for this paper are available at *Journal of Petrology* online.

REFERENCES

Agranier, A., Lee, C.-T. A., Li, Z.-X. A. & Leeman, W. P. (2007). Fluid-mobile element budgets in serpentinized oceanic lithospheric mantle: Insights from B, As, Li, Pb, PGEs and Os isotopes in the Feather River Ophiolite, California. *Chemical Geology* **245**, 230–241.

Auzende, A.-L., Guillot, S., Devouard, B. & Baronnet, A. (2006). Serpentinites in an Alpine convergent setting: Effects of metamorphic grade and deformation on microstructures. *European Journal of Mineralogy* **18**, 21–33.

Bach, W., Erzinger, J., Alt, J. C. & Teagle, D. A. H. (1996). Chemistry of the lower sheeted dike complex, Hole 504B, Leg 148: the influence of magmatic differentiation and hydrothermal alteration. In: Alt, J. C., Kinoshita, H., Stokking, L. B. & Michael, P. J. (eds) *Proceedings of the Ocean Drilling Program, Scientific Results, 148.* College Station, TX: Ocean Drilling Program, pp. 39–55.

Barnicoat, A. C. & Cartwright, I. (1997). The gabbro–eclogite transformation: an oxygen isotope and petrographic study of west Alpine ophiolites. *Journal of Metamorphic Geology* **15**, 93–104.

Becker, H., Jochum, K. P. & Carlson, R. W. (1999). Constraints from high-pressure veins in eclogites on the composition of hydrous fluids in subduction zones. *Chemical Geology* **160**, 291–308.

Blake, M. C., Moore, D. E. & Jayko, A. S. (1995). The role of serpentinite mélange in the unroofing of UHPM rocks: an example from western Alps of Italy. In: Coleman, R. G. & Wang, X. (eds) *Ultrahigh Pressure Metamorphism.* Cambridge: Cambridge University Press, pp. 182–205.

Blichert-Toft, J. & Albarède, F. (1997). The Lu–Hf isotope geochemistry of chondrites and the evolution of the mantle–crust system. *Earth and Planetary Science Letters* **148**, 243–258.

Bons, P. D. (2001). The formation of large quartz veins by rapid ascent of fluids in mobile hydrofractures. *Tectonophysics* **336**, 1–17.

Carmichael, I. S. E. (1964). The petrology of Thingmuli, a Tertiary volcano in eastern Iceland. *Journal of Petrology* **5**, 435–460.

Chauvel, C. & Blichert-Toft, J. (2001). A hafnium isotope and trace element perspective on melting of the depleted mantle. *Earth and Planetary Science Letters* **190**, 137–151.

Cheng, H., Nakamura, E., Kobayashi, K. & Zhou, Z. (2007). Origin of atoll garnets in eclogites and implications for the redistribution of trace elements during slab exhumation in a continental subduction zone. *American Mineralogist* **92**, 1119–1129.

Cliff, R. A., Barnicoat, A. C. & Inger, S. (1998). Early Tertiary eclogite facies metamorphism in the Monviso Ophiolites. *Journal of Metamorphic Geology* **16**, 447–455.

Compagnoni, R., Ferraris, G. & Mellini, M. (1985). Carlosturanite, a new asbestiform rock-forming silicate from Val Varaita, Italy. *American Mineralogist* **70**, 767–772.

Connolly, J. A. D. & Podladchikov, Y. (1998). Compaction-driven fluid flow in viscoelastic rock. *Geodinamica Acta* **11**, 55–84.

Davies, J. H. (1999). The role of hydraulic fractures and intermediate-depth earthquakes in generating subduction-zone magmatism. *Nature* **398**, 142–145.

Duchêne, S., Blichert-Toft, J., Luais, B., Télouk, P., Lardeaux, J.-M. & Albarède, F. (1997). The Lu–Hf dating of garnets and the ages of the Alpine high-pressure metamorphism. *Nature* **387**, 586–589.

Durrant, S. F. (1994). Feasibility of improvement in analytical performance in laser-ablation inductively-coupled plasma-mass spectrometry (LA-ICP-MS) by addition of nitrogen to the argon plasma. *Fresenius' Journal of Analytical Chemistry* **349**, 768–771.

Eggins, S. M., Rudnick, R. L. & McDonough, W. F. (1998). The composition of peridotites and their minerals: a laser ablation ICP-MS study. *Earth and Planetary Science Letters* **154**, 53–71.

Ferrando, S., Frezzotti, M. L., Petrelli, M. & Compagnoni, R. (2009). Metasomatism of continental crust during subduction: the UHP whiteschists from Southern Dora-Maira Massif (Italian Western Alps). *Journal of Metamorphic Geology* **27**, 739–756.

Gao, J., John, T., Klemd, R. & Xiong, X. (2007). Mobilization of Ti–Nb–Ta during subduction: Evidence from rutile-bearing dehydration segregations and veins hosted in eclogite, Tianshan, NW China. *Geochimica et Cosmochimica Acta* **71**, 4974–4996.

Green, T. H. & Adam, J. (2003). Experimentally-determined trace element characteristics of aqueous fluid from partially dehydrated mafic oceanic crust at 3·0 GPa, 650–700°C. *European Journal of Mineralogy* **15**, 815–830.

Groppo, C. & Compagnoni, R. (2007). Metamorphic veins from serpentinites of the Piemonte Zone, western Alps, Italy: a review. *Periodico di Mineralogia* **76**, 127–153.

Hacker, B. R., Peacock, S. M., Abers, G. A. & Holloway, S. D. (2003). Subduction factory 2. Are intermediate-depth earthquakes in subducting slabs linked to metamorphic dehydration reactions? *Journal of Geophysical Research* **108**, article no. 2030.

Harlow, G. E. & Olds, E. P. (1987). Observations on terrestrial ureyite and ureyitic pyroxene. *American Mineralogist* **72**, 126–136.

Hart, S. R., Erlank, A. J. & Kable, E. J. D. (1974). Sea floor basalt alteration: some chemical and Sr isotope effects. *Contributions to Mineralogy and Petrology* **44**, 219–230.

Hattori, K. H. & Guillot, S. (2007). Geochemical character of serpentinites associated with high- to ultrahigh-pressure metamorphic rocks in the Alps, Cuba, and the Himalayas: Recycling of elements in subduction zones. *Geochemistry, Geophysics, Geosystems* **8**, doi:10.1029/2007GC001594.

Hermann, J. & Spandler, C. (2008). Sediment melts at sub-arc depths: an experimental study. *Journal of Petrology* **49**, 717–740.

Hermann, J., Spandler, C., Hack, A. & Korsakov, A. V. (2006). Aqueous fluids and hydrous melts in high-pressure and ultra-high pressure rocks: Implications for element transfer in subduction zones. *Lithos* **92**, 399–417.

Hiess, J., Bennett, V. C., Nutman, A. P. & Williams, I. S. (2009). *In situ* U–Pb, O and Hf isotopic compositions of zircon and olivine from Eoarchaean rocks, West Greenland: New insights to making old crust. *Geochimica et Cosmochimica Acta* **73**, 4489–4516.

Hoskin, P. W. O. & Schaltegger, U. (2003). The composition of zircon and igneous and metamorphic petrogenesis. In: Hanchar, J. M. & Hoskin, P. W. O. (eds) *Zircon. Mineralogical Society of America and Geochemical Society, Reviews in Mineralogy and Geochemistry* **53**, 27–62.

Ikehata, K. & Arai, S. (2004). Metasomatic formation of kosmochlor-bearing diopside in peridotite xenoliths from North Island, New Zealand. *American Mineralogist* **89**, 1396–1404.

John, T. & Schenk, V. (2006). Interrelations between intermediate-depth earthquakes and fluid flow within subducting oceanic plates: constraints from eclogite-facies pseudotachylytes. *Geology* **34**, 557–560.

John, T., Scherer, E. E., Haase, K. & Schenk, V. (2004). Trace element fractionation during fluid-induced eclogitization in a subducting slab: trace element and Lu–Hf–Sm–Nd isotope systematics. *Earth and Planetary Science Letters* **227**, 441–456.

John, T., Klemd, R., Gao, J. & Garbe-Schoenberg, C.-D. (2008). Trace-element mobilization in slabs due to non steady-state fluid–rock interaction: Constraints from an eclogite-facies transport vein in blueschist (Tianshan, China). *Lithos* **103**, 1–24.

Kelemen, P. B., Hanghoj, K. & Greene, A. R. (2003). One view of the geochemistry of subduction-related magmatic arcs, with emphasis on primitive andesite and lower crust. In: Rudnick, R. L. (ed.) *The Crust. Treatise on Geochemistry*. Oxford: Elsevier–Pergamon, pp. 593–659.

Kessel, R., Schmidt, M. W., Ulmer, P. & Pettke, T. (2005). Trace element signature of subduction-zone fluids, melts and supercritical liquids at 120–180 km depth. *Nature* **437**, 724–727.

Klein, E. M. (2003). Geochemistry of the igneous oceanic crust. In: Rudnick, R. L. (ed.) *The Crust. Treatise on Geochemistry*. Oxford: Elsevier–Pergamon, pp. 433–464.

Klimm, K., Blundy, J. D. & Green, T. H. (2008). Trace element partitioning and accessory phase saturation during H_2O-saturated melting of basalt with implications for subduction zone chemical fluxes. *Journal of Petrology* **49**, 523–553.

Kogiso, T., Tatsumi, Y. & Nakano, S. (1997). Trace element transport during dehydration processes in the subducted oceanic crust: 1. Experiments and implications of the origin of ocean island basalts. *Earth and Planetary Science Letters* **148**, 193–205.

Kroslakova, I. & Gunther, D. (2007). Elemental fractionation in laser ablation-inductively coupled plasma-mass spectrometry: evidence for mass load induced matrix effects in the ICP during ablation of a silicate glass. *Journal of Analytical Atomic Spectrometry* **22**, 51–62.

Lambert, I. B. & Wyllie, P. J. (1972). Melting of gabbro (quartz eclogite) with excess water to 35 kilobars, with geological applications. *Journal of Geology* **80**, 693–708.

Lardeaux, J. M., Nisio, P. & Boudeulle, M. (1987). Deformational and metamorphic history at the Lago Superiore area of the Monviso ophilitic complex (Italian Western Alps). *Ophioliti* **12**, 479–502.

Lombardo, B., Nervo, R., Compagnoni, R., Messiga, B., Kienast, J. R., Mevel, C., Fiora, L., Piccardo, G. B. & Lanza, R. (1978). Osservazioni preliminari sulle ofioliti metamorfiche del Monviso (Alpi Occidentali). *Rendiconti della Societa Italiana di Mineralogia e Petrologia* **34**, 253–305.

Lombardo, B., Rubatto, D. & Castelli, D. (2002). Ion microprobe U–Pb dating of zircon from a Monviso metaplagiogranite: implications for the evolution of the Piedmont–Liguria Tethys in the Western Alps. *Ofioliti* **27**, 109–117.

López-Sánchez Vizcaíno, V., Gómez-Pugnaire, M. T., Garrido, C., Padrón-Navarta, J. A. & Mellini, M. (2009). Breakdown mechanisms of titanclinohumite in antigorite serpentinite (Cerro del Almirez massif, S. Spain): a petrological and TEM study. *Lithos* **107**, 216–226.

Manning, C. E. (2004). The chemistry of subduction-zone fluids. *Earth and Planetary Science Letters* **223**, 1–16.

Martin, A. J. (2009). Sub-millimeter heterogeneity of yttrium and chromium during growth of semi-pelitic garnet. *Journal of Petrology* **50**, 1713–1727.

Messiga, B., Kienast, J. R., Rebay, G., Riccardi, M. P. & Tribuzio, R. (1999). Cr-rich magnesiochloritoid eclogites from the Monviso ophiolites (Western Alps, Italy). *Journal of Metamorphic Geology* **17**, 287–299.

Miller, J. A. & Cartwright, I. (2000). Distinguishing between seafloor alteration and fluid flow during subduction using stable isotope geochemistry: examples from Tethyan ophiolites in the Western Alps. *Journal of Metamorphic Geology* **18**, 467–482.

MONVISO (1980). The Monviso ophiolite complex. In: Panajotou, A. (ed.) *Proceedings of the International Ophiolite Symposium*. Nicosia: Geological Survey Department, pp. 332–340.

Nadeau, S., Philippot, P. & Pineau, F. (1993). Fluid inclusion and mineral isotopic compositions (H–C–O) in eclogitic rocks as tracers of local fluid migration during high-pressure metamorphism. *Earth and Planetary Science Letters* **114**, 431–448.

Natland, J. H., Meyer, P. S., Dick, H. J. B. & Bloomer, S. H. (1991). Magmatic oxides and sulfides in gabbroic rocks from ODP Hole 735B and the later development of the liquid line of descent. In: Von Herzen, R. P. & Robinson, P. T. *et al.* (eds) *Proceeding of the Ocean Drilling Program, Scientific Results, 118.* College Station, TX: Ocean Drilling Program, pp. 75–112.

Nishiyama, T., Uehara, S. & Shinno, I. (1986). Chromian omphacite from low-grade metamorphic rocks, Nishisonogi, Kyushu, Japan. *Journal of Metamorphic Geology* **4**, 69–78.

Oliver, N. H. S. & Bons, P. D. (2001). Mechanisms of fluid flow and fluid–rock interaction in fossil metamorphic hydrothermal systems inferred from vein–wallrock pattern, geometry and microstructure. *Geofluids* **1**, 137–162.

Ozawa, K., Meyer, P. S. & Bloomer, S. H. (1991). Mineralogy and textures of iron–titanium oxide gabbros and associated olivine gabbros from Hole 735B. In: Von Herzen, R. P. & Robinson, P. T. *et al.* (eds) *Proceeding of the Ocean Drilling Program, Scientific Results, 118.* College Station, TX: Ocean Drilling Program, pp. 41–73.

Peacock, S. M. (1993). The importance of blueschist to eclogite dehydration reactions in subducting oceanic crust. *Geological Society of America Bulletin* **105**, 684–694.

Peacock, S. M. (2001). Are the lower planes of double seismic zones caused by serpentine dehydration in subducting oceanic mantle? *Geology* **29**, 299–302.

Perfit, M. R. & Fornari, D. J. (1983). Geochemical studies of abyssal lavas recovered by DSRV *Alvin* from Eastern Galapagos Rift, Inca Transform, and Ecuador Rift 2. Phase chemistry and crystallization history. *Journal of Geophysical Research* **88**, 10530–10550.

Pettke, T. (2008). Analytical protocols for element concentration and isotope ratio measurements in fluid inclusions by LA-(MC)-ICP-MS. In: Sylvester, P. (ed.) *Laser Ablation ICP-MS in the Earth Sciences: Current Practices and Outstanding Issues. Mineralogical Association of Canada, Short Course Series* **40**, 189–218.

Philippot, P. (1987). 'Crack-seal' vein geometry in eclogitic rocks. *Geodinamica Acta* **1**, 171–181.

Philippot, P. (1993). Fluid–melt–rock interaction in mafic eclogites and coesite-bearing metasediments: Constraints on volatile recycling during subduction. *Chemical Geology* **108**, 93–112.

Philippot, P. & Kienast, J. R. (1989). Chemical–microstructural changes in eclogitic shear zones, Monviso (Western Alps), as indicators of strain history, mechanisms and scales of mass transfer. *Lithos* **23**, 179–200.

Philippot, P. & Selverstone, J. (1991). Trace-element-rich brines in eclogitic veins: implications for fluid composition and transport during subduction. *Contributions to Mineralogy and Petrology* **106**, 417–430.

Philippot, P. & Van Roermund, H. L. M. (1992). Deformation processes in eclogitic rocks: evidence for the rheological delamination of the oceanic crust in deeper levels of subduction zones. *Journal of Structural Geology* **14**, 1059–1077.

Philippot, P., Agrinier, P. & Scambelluri, M. (1998). Chlorine cycling during subduction of altered oceanic crust. *Earth and Planetary Science Letters* **161**, 33–44.

Poli, S. & Schmidt, M. W. (2002). Petrology of subducted slabs. *Annual Review of Earth and Planetary Sciences* **30**, 207–235.

Rubatto, D. & Hermann, J. (2003). Zircon formation during fluid circulation in eclogites (Monviso, Western Alps): implications for Zr and Hf budget in subduction zones. *Geochimica et Cosmochimica Acta* **67**, 2173–2187.

Savov, I. P., Ryan, J. G., D'Antonio, M., Kelley, K. & Mattie, P. (2005). Geochemistry of serpentinized peridotites from the Mariana Forearc Conical Seamount, ODP Leg 125: Implications for the elemental recycling at subduction zones. *Geochemistry, Geophysics, Geosystems* **6**, doi:10.1029/2004GC000777.

Scambelluri, M. & Philippot, P. (2001). Deep fluids in subduction zones. *Lithos* **55**, 213–227.

Scambelluri, M., Pennacchioni, G. & Philippot, P. (1998). Salt-rich aqueous fluids formed during eclogitization of metabasites in the Alpine continental crust (Austroalpine Mt. Emilius unit, Italian western Alps). *Lithos* **43**, 151–167.

Scambelluri, M., Rampone, E. & Piccardo, G. B. (2001). Fluid and element cycling in subducted serpentinite: a trace element study of the Erro–Tobbio high-pressure ultramafites (Western Alps, NW Italy). *Journal of Petrology* **42**, 55–67.

Scambelluri, M., Fiebig, J., Malaspina, N., Müntener, O. & Pettke, T. (2004). Serpentinite subduction: Implications for fluid processes and trace element recycling. *International Geology Review* **46**, 595–613.

Schmidt, M. W. & Poli, S. (1998). Experimentally based water budgets for dehydrating slabs and consequences for arc magma generation. *Earth and Planetary Science Letters* **163**, 361–379.

Schwartz, S., Lardeaux, J.-M., Guillot, S. & Tricart, P. (2000). Diversité du métamophism éclogitique dans le massif ophiolitique du Monviso (Alpes occidentales, Italie). *Geodinimica Acta* **13**, 169–188.

Schwartz, S., Allemand, P. & Guillot, S. (2001). Numerical model of the effect of serpentinites on the exhumation of eclogitic rocks: insights from the Monviso ophiolitic massif (Western Alps). *Tectonophysics* **342**, 193–206.

Smith, D. & Griffin, W. L. (2005). Garnetite xenoliths and mantle–water interactions below the Colorado Plateau, southwestern United States. *Journal of Petrology* **46**, 1901–1924.

Söderlund, U., Patchett, P. J., Vervoort, J. D. & Isachsen, C. E. (2004). The ^{176}Lu decay constant determined by Lu–Hf and U–Pb isotope systematics of Precambrian mafic intrusions. *Earth and Planetary Science Letters* **219**, 311–324.

Sorensen, S. S. & Grossman, J. N. (1983). Accessory minerals and subduction zone metasomatism: a geochemical comparison of two mélanges (Washington and California, U.S.A.). *Chemical Geology* **110**, 269–297.

Spandler, C. & Hermann, J. (2006). High-pressure veins in eclogite from New Caledonia and their significance for fluid migration and seismic activity in subduction zones. *Lithos* **89**, 135–153.

Spandler, C., Mavrogenes, J. M. & Hermann, J. (2007). Experimental constraints on element mobility from subducted sediments using high-*P* synthetic fluid/melt inclusions. *Chemical Geology* **239**, 228–249.

Spandler, C., Hermann, J., Faure, K., Mavrogenes, J. A. & Arculus, R. J. (2008). The importance of talc and chlorite 'hybrid' rocks for volatile recycling through subduction zones; evidence from the high-pressure subduction mélange of New Caledonia. *Contributions to Mineralogy and Petrology* **155**, 181–198.

Spandler, C., Pettke, T. & Hermann, J. (2009). The composition of serpentinite dehydration fluids in subduction zones: an experimental study. *Geochimica et Cosmochimica Acta* **73**, Supplement 1, A1256.

Stern, R. J. (2002). Subduction zones. *Reviews of Geophysics* **40**, doi:10.1029/2001RG000108.

Sun, S. S. & McDonough, W. F. (1989). Chemical and isotopic systematics of oceanic basalts; implications for mantle composition and processes. In: Saunders, A. D. & Norry, M. J. (eds) *Magmatism in the Ocean Basins. Geological Society, London, Special Publications* **42**, 313–345.

Taylor, S. R. & McLennan, S. M. (1985). *The Continental Crust: its Composition and Evolution*. Oxford: Blackwell, 312 p.

Tenthorey, E. & Hermann, J. (2004). Composition of fluids during serpentinite breakdown in subduction zones: Evidence for limited boron mobility. *Geology* **32**, 865–868.

Thirlwall, M. F. & Anczkiewicz, R. (2004). Multidynamic isotope ratio analysis using MC–ICP–MS and the causes of secular drift in Hf, Nd and Pb isotope ratios. *International Journal of Mass Spectroscopy* **235**, 59–81.

Tsujimori, T. & Liou, J. G. (2004). Coexisting chromian omphacite and diopside in tremolite schist from the Chugoku Mountains, SW Japan: The effect of Cr on the omphacite–diopside immiscibility gap. *American Mineralogist* **89**, 7–14.

Ulmer, P. & Trommsdorff, V. (1999). Phase relations of hydrous mantle subducting to 300 km. In: Fei, Y., Bertka, N. & Mysen, B. O. (eds) *Mantle Petrology: Field Observations and High-pressure Experimentation. Geochemical Society Special Publication* **6**, 259–281.

Van der Straaten, F., Schenk, V., John, T. & Gao, J. (2008). Blueschist-facies rehydration of eclogites (Tian Shan, NW China): Implications for fluid–rock interaction in the subduction channel. *Chemical Geology* **255**, 195–219.

Wang, C. Y., Campbell, I. H., Allen, C. M., Williams, I. S. & Eggins, S. M. (2009). Rate of growth of the preserved North American continental crust: Evidence from Hf and O isotopes in Mississippi detrital zircons. *Geochimica et Cosmochimica Acta* **73**, 712–728.

Widmer, T. & Thompson, A. B. (2001). Local origin of high pressure vein material in eclogite facies rocks of the Zermatt–Saas Zone, Switzerland. *American Journal of Science* **301**, 627–656.

Wood, D. A. (1978). Major and trace element variations in the Tertiary lavas of eastern Iceland and their significance with respect to the Iceland geochemical anomaly. *Journal of Petrology* **19**, 393–436.

Zack, T. & John, T. (2007). An evaluation of reactive fluid flow and trace-element mobility in subducting slabs. *Chemical Geology* **239**, 199–216.

Zack, T., Kronz, A., Foley, S. F. & Rivers, T. (2002). Trace element abundances in rutiles from eclogites and associated garnet mica schists. *Chemical Geology* **184**, 97–122.

Zhang, Z.-M., Shen, K., Sun, W.-D., Liu, Y.-S., Liou, J. G., Shi, C. & Wang, J.-J. (2008). Fluids in deeply subducted continental crust : Petrology, mineral chemistry and fluid inclusion of UHP metamorphic veins from the Sulu orogen, eastern China. *Geochimica et Cosmochimica Acta* **72**, 3200–3228.

Zheng, Y. F., Wu, Y.-B., Zhao, Z.-F., Zhang, S.-B., Xu, P. & Wu, F.-Y. (2005). Metamorphic effect on zircon Lu–Hf and U–Pb isotope systems in ultrahigh-pressure eclogite-facies metagranite and metabasalt. *Earth and Planetary Science Letters* **240**, 378–400.